



HAL
open science

Amplified Fluorescence in Situ Hybridization by Small and Bright Dye-Loaded Polymeric Nanoparticles

Sylvie Egloff, Nina Melnychuk, Elisabete Cruz da Silva, Andreas Reisch, Sophie Martin, Andrey S Klymchenko

► **To cite this version:**

Sylvie Egloff, Nina Melnychuk, Elisabete Cruz da Silva, Andreas Reisch, Sophie Martin, et al.. Amplified Fluorescence in Situ Hybridization by Small and Bright Dye-Loaded Polymeric Nanoparticles. ACS Nano, 2021, 16 (1), pp.1381 - 1394. 10.1021/acsnano.1c09409 . hal-04292567

HAL Id: hal-04292567

<https://hal.science/hal-04292567v1>

Submitted on 17 Nov 2023

HAL is a multi-disciplinary open access archive for the deposit and dissemination of scientific research documents, whether they are published or not. The documents may come from teaching and research institutions in France or abroad, or from public or private research centers.

L'archive ouverte pluridisciplinaire **HAL**, est destinée au dépôt et à la diffusion de documents scientifiques de niveau recherche, publiés ou non, émanant des établissements d'enseignement et de recherche français ou étrangers, des laboratoires publics ou privés.

Amplified Fluorescence *in Situ* Hybridization by Small and Bright Dye-Loaded Polymeric Nanoparticles

Sylvie Egloff,[§] Nina Melnychuk,[§] Elisabete Cruz Da Silva, Andreas Reisch, Sophie Martin, and Andrey S. Klymchenko*



Cite This: <https://doi.org/10.1021/acsnano.1c09409>



Read Online

ACCESS |



Metrics & More



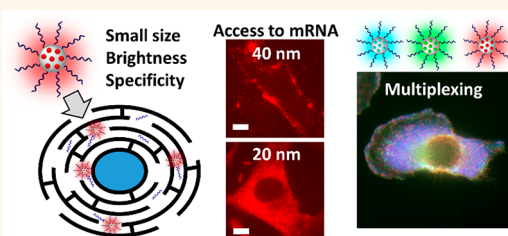
Article Recommendations



Supporting Information

ABSTRACT: Detection and imaging of RNA at the single-cell level is of utmost importance for fundamental research and clinical diagnostics. Current techniques of RNA analysis, including fluorescence *in situ* hybridization (FISH), are long, complex, and expensive. Here, we report a methodology of amplified FISH (AmpliFISH) that enables simpler and faster RNA imaging using small and ultrabright dye-loaded polymeric nanoparticles (NPs) functionalized with DNA. We found that the small size of NPs (below 20 nm) was essential for their access to the intracellular mRNA targets in fixed permeabilized cells. Moreover, proper selection of the polymer matrix of DNA-NPs minimized nonspecific intracellular interactions. Optimized DNA-NPs enabled sequence-specific imaging of different mRNA targets (survivin, actin, and polyA tails), using a simple 1 h staining protocol. Encapsulation of cyanine and rhodamine dyes with bulky counterions yielded green-, red-, and far-red-emitting NPs that were 2–100-fold brighter than corresponding quantum dots. These NPs enabled multiplexed detection of three mRNA targets simultaneously, showing distinctive mRNA expression profiles in three cancer cell lines. Image analysis confirmed the single-particle nature of the intracellular signal, suggesting single-molecule sensitivity of the method. AmpliFISH was found to be semiquantitative, correlating with RT-qPCR. In comparison with the commercial locked nucleic acid (LNA)-based FISH technique, AmpliFISH provides 8–200-fold stronger signal (dependent on the NP color) and requires only three steps *vs* ~20 steps together with a much shorter time. Thus, combination of bright fluorescent polymeric NPs with FISH yields a fast and sensitive single-cell transcriptomic analysis method for RNA research and clinical diagnostics.

KEYWORDS: fluorescent nanoparticles, DNA-functionalized polymeric nanoparticles, fluorescence *in situ* hybridization, single-cell analysis, RNA imaging, mRNA, fluorescence microscopy



With the ever-growing role of RNA in understanding and controlling cellular processes,^{1,2} detection and imaging of intracellular RNA attract significant attention.^{3–5} Current approaches include fluorescence *in situ* hybridization (FISH),⁶ single-cell RNA sequencing,^{7,8} and molecular biology techniques based on labeled RNA-binding proteins^{4,9} and light-up aptamers.^{10–14} *In situ* hybridization, introduced more than 50 years ago,^{15,16} and its fluorescence version FISH^{17,18} are particularly suitable for imaging native nucleic acids within cells and tissues, with applications ranging from fundamental RNA research to clinical diagnostics.^{6,19} In particular, RNA-FISH, which allows spatial and temporal monitoring of intracellular RNA, provides important insights into mechanisms of transcription and translation^{20,21} and serves as a tool for cell-based diagnostics.^{22,23} Advanced versions of RNA-FISH, developed in the last decades, enable detection and quantification of intracellular RNA with single-molecule sensitivity.^{24–27} Nevertheless, broad applications of RNA-

FISH in research and clinical diagnostics are still limited by a number of challenges. In particular, low-abundant RNA are still difficult to identify,²⁸ because of limited fluorescence signal provided by single organic dye molecules. Therefore, many approaches have been developed to amplify the fluorescence signal, such as branched DNA amplification,^{29–31} different isothermal amplification strategies,³² rolling circle amplification (RPA),³³ hybridization chain reaction (HCR),^{34,35} primer-exchange reaction,^{36,37} and click-amplifying FISH (Clamp-FISH).³⁸ The signal amplification can be also achieved by using

Received: October 24, 2021

Accepted: December 14, 2021

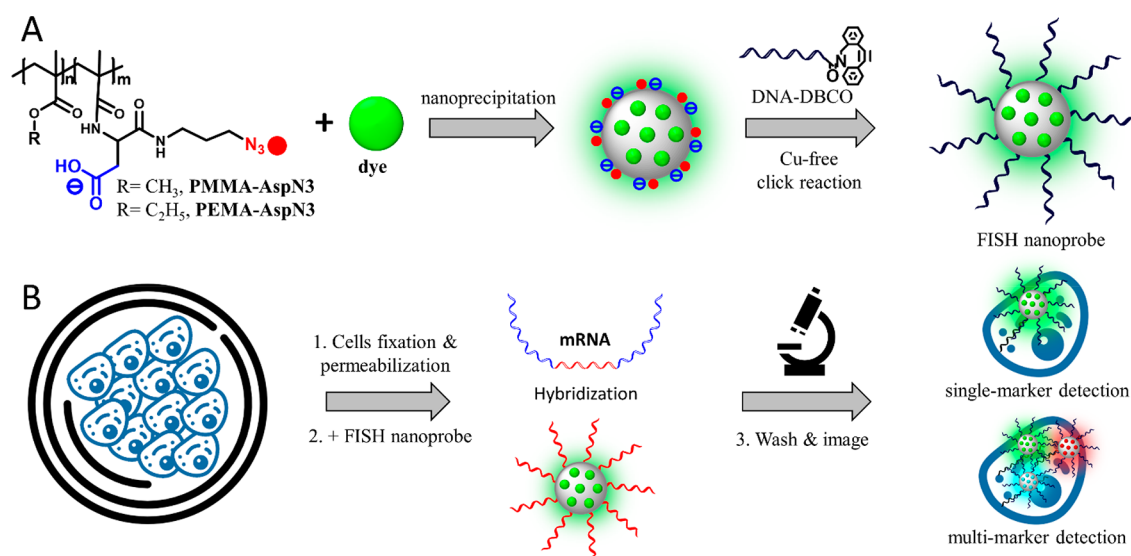


Figure 1. Principle of AmpliFISH using DNA-functionalized dye-loaded polymeric NPs. (A) Design of FISH nanoprobe based on polymeric nanoparticles. (B) Workflow for detection of target mRNA in fixed and permeabilized cells.

multiple singly labeled oligonucleotides (generally 30–48) that hybridize along the same target RNA transcript,²⁷ known as the Stellaris FISH method.³⁹ However, FISH techniques include complicated time-consuming procedures with multiple steps and require experienced staff, which make development of validated protocols for clinics very expensive.⁴⁰ Moreover, FISH protocols are probe- and sample-dependent and have to be optimized for each set of conditions.⁴¹

Fluorescent probes based on nanoparticles (NPs) can potentially overcome some of the limitations in the field of nucleic acid detection.⁴² In particular, high fluorescence brightness of NPs may allow direct detection of the biomolecular targets without the need of complex and time-consuming amplification protocols.^{43–48} NPs can provide fluorescence signal amplification for nucleic acid detection using different mechanisms, including energy transfer from semiconductor quantum dots⁴⁹ and polymeric NPs^{50–52} as well as plasmonics-based fluorescence enhancement,^{53,54} hybridization-triggered molecular assembly,⁵⁵ *etc.* Direct intracellular detection of nucleic acids by NPs inside the cells is a highly attractive approach,⁵⁶ and a few reported examples include gold nanoparticles (nanoflares)^{57–59} DNA-based nanostructures,^{60–63} semiconductor quantum dots,^{64,65} upconversion NPs,⁶⁶ carbon nanostructures,^{67,68} as well as lipid NPs,^{69,70} polymeric NPs,⁷¹ hybrid organic–inorganic NPs,⁷² *etc.* However, RNA detection in live cells remains complicated by efficient endocytosis of nanomaterials with their potential degradation by enzymes and generic problem of endosomal escape of entrapped NPs.^{73–75} In this respect, the combination of the FISH technique in fixed and permeabilized cells with luminescent NPs is of particular interest, because it can ensure direct access of NPs to the target RNA and take advantage of established FISH protocols in biological and clinical applications.¹⁹ However, this possibility was realized only recently using semiconductor quantum dots (QDs) in combination with the Stellaris approach, where distinct mRNA transcripts have been detected and quantified at the single-molecule level in individual cells.⁶⁵ To achieve this, the authors specially designed compact QDs, which could better access the whole cytosol and thus hybridize with the intracellular mRNA.⁶⁵

Dye-loaded polymeric nanoparticles, which have attracted 95 attention in recent years due to their high brightness and 96 modularity,^{45,76} could be a promising platform for development 97 of a simple and rapid RNA-FISH probes. To address the 98 problem of aggregation-caused quenching of encapsulated dyes 99 in these NPs, we proposed a concept of ionic dye insulation by 100 bulky hydrophobic counterions, yielding NPs 6–100-fold 101 brighter than corresponding QDs.^{52,77,78} The size of these 102 NPs can be tuned from 10 to 50 nm depending on the nature of 103 the polymer,⁷⁹ which is a critical point because NPs should be 104 able to reach the RNA target within the cytosol.⁶⁵ Indeed, 105 polymeric NPs with sizes of <23 nm are required to diffuse and 106 spread in the cytosol of living cells.⁸⁰ In addition to rhodamine 107 dye, cyanine dyes can also be encapsulated to prepare NPs of any 108 desired color, which was applied for multicolor barcoding of live 109 cells and for long-term tracking *in vitro* and *in vivo*.⁸¹ Moreover, 110 the efficient energy transfer within donor dyes inside the NPs 111 can generate a giant light-harvesting antenna that amplifies the 112 fluorescence signal of a single acceptor >1000-fold.⁸² Their 113 functionalization with oligonucleotides yielded nanoprobe for 114 amplified detection of DNA and RNA in solutions with a 115 picomolar limit of detection⁵² and on surfaces with single- 116 molecule sensitivity⁵¹ and compatibility with mobile phone 117 cameras.⁸³ These DNA-functionalized NPs have already been 118 validated for detection of microRNA in cell extracts,⁸⁴ but they 119 have not been explored to date for direct detection of RNA 120 inside the cells. 121

In the present work, we developed a methodology of amplified 122 FISH (AmpliFISH) based on ultrabright dye-loaded polymeric 123 NPs functionalized with DNA. In this approach, the hybrid- 124 ization AmpliFISH probe with the target mRNA inside the cells 125 results in a fluorescence signal equivalent to 80–300 126 encapsulated dyes per single sequence, which ensures strong 127 signal amplification. We show that the size of NPs < 16 nm was 128 essential to achieve effective penetration of fixed cells and 129 hybridization with the target. Owing to their high brightness, 130 these FISH nanoprobe can detect target mRNA in fixed cells 131 using a simple and rapid protocol (<3 h). Importantly, FISH 132 nanoprobe of three different colors could be used simulta- 133 neously to target different RNA sequences. The methodology 134

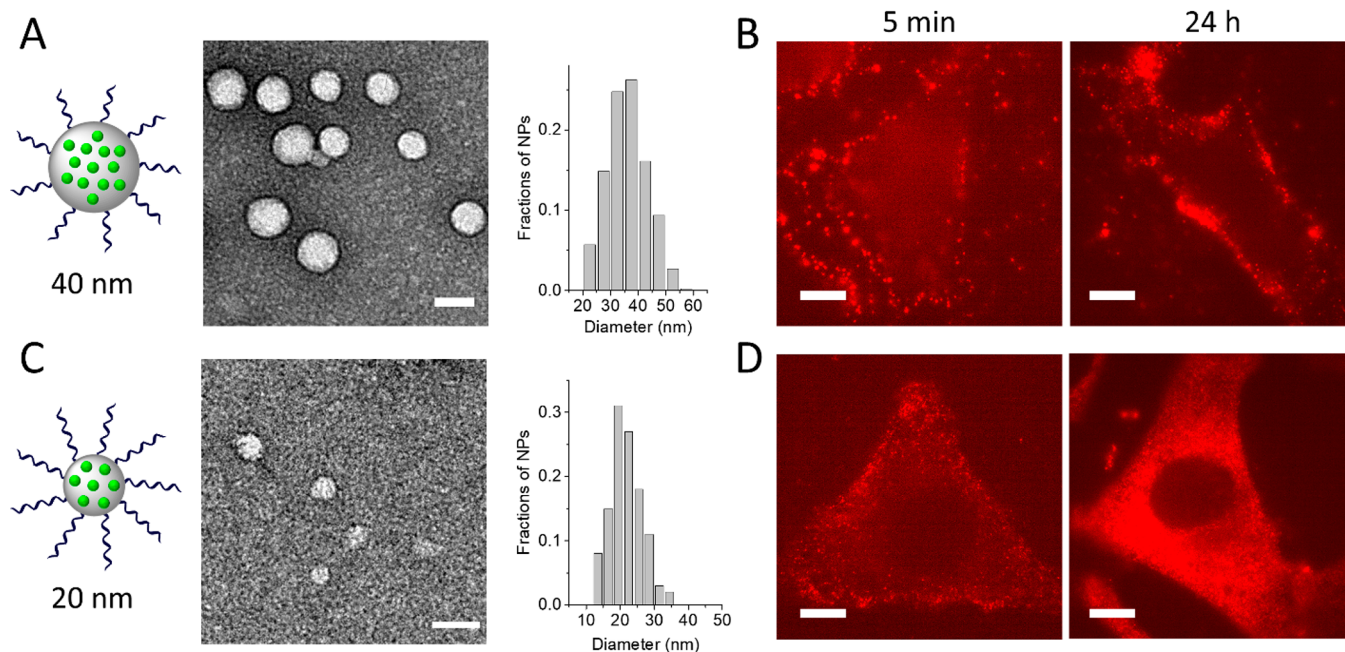


Figure 2. Testing DNA-functionalized NPs of two different sizes in fixed permeabilized HeLa cells. (A, C) NPs of two different average sizes of their core, ~ 40 nm (A) and ~ 20 nm (C), and their corresponding TEM images and size distribution histograms. (B, D) Fluorescence microscopy (TIRF) images of cells labeled for different times (5 min and 24 h) with DNA-NPs (T20-NPs) of two different sizes: ~ 40 nm (B) and ~ 20 nm (D). Scale bar is $10 \mu\text{m}$.

135 was validated on three cancer cell lines, and it allows
 136 semiquantitative analysis of mRNA abundance. The developed
 137 probes and the FISH methodology can greatly simplify FISH-
 138 based imaging of RNA inside cells for both fundamental research
 139 and clinical diagnostics.

140 RESULTS AND DISCUSSION

141 **Design and Optimization of FISH Nanoprobes.** The
 142 design of our FISH nanoprobes is based on dye-loaded
 143 polymeric NPs functionalized with nucleic acids complementary
 144 to the mRNA target (Figure 1). Dye-loaded NPs are made of
 145 poly(methyl methacrylate) (PMMA) or poly(ethyl methacry-
 146 late) (PEMA) polymers bearing azide and a negatively charged
 147 carboxylate group (Figure 1A). Nanoprecipitation of these
 148 hydrophobic polymers with charged groups yields ultrasmall
 149 NPs, where the core is formed by the hydrophobic domain of the
 150 polymer, while the charged carboxylate exposes an azide group
 151 at the NP surface to ensure high reactivity for the click
 152 reaction.^{51,52,85} For encapsulation, we used octadecyl rhod-
 153 amine B R18 with its bulky hydrophobic counterion trakis-
 154 (pentafluorophenyl)borate (F5). The latter serves as an
 155 insulator that prevents the dyes from aggregation-caused
 156 quenching when loaded at high concentration and at the same
 157 time ensures effective encapsulation without dye leakage.^{77,86}
 158 The dye-loaded NPs were obtained by nanoprecipitation of the
 159 polymer and the dye from acetonitrile into corresponding buffer.
 160 Then, oligonucleotides were grafted to the NPs' surface by
 161 reacting the exposed azide groups with DBCO groups of
 162 oligonucleotides (Figure 1A). The sequence of grafted
 163 oligonucleotides was a 20–22mer complementary to the target
 164 mRNA of actin and survivin. The former is a common
 165 housekeeping gene well expressed in many cell lines, while the
 166 latter is a common marker of cancer cells.⁸⁷ In our AmpliFISH
 167 technique, the NPs bearing capture sequences are expected to
 168 hybridize with the mRNA target inside the cells. For this

purpose, the cells should be fixed and permeabilized (Figure
 169 1B). 170

The key question here is the size of NPs required to penetrate
 171 the cells, diffuse freely through the labyrinth of the intracellular
 172 structures, and reach the target mRNA sequence.⁶⁵ Therefore,
 173 we first formulated dye-loaded NPs with different sizes. The
 174 larger particles (40 nm core size, Figure 2A) were based on a
 175 PMMA bearing 1.6% of charged groups (PMMA-AspN3-1.6%),
 176 the same as reported previously by us.⁵² To obtain smaller NPs,
 177 we used PMMA with a larger number of charged groups (5%),
 178 which was shown to favor a decrease in the particle size obtained
 179 by nanoprecipitation.^{51,80} The obtained NPs loaded with 30 wt
 180 % of R18/F5 displayed a 22 nm core size according to
 181 transmission electron microscopy (TEM, Figure 2C). 182

To verify whether the probes can enter fixed permeabilized
 183 cells and hybridize with mRNA, we first functionalized NPs with
 184 T20 DNA. They are expected to hybridize with all mRNA,
 185 because each mRNA bears a poly(A) tail at the 3' end. After
 186 fixation and permeabilization, the cells were incubated with NPs
 187 (30 min), then washed and imaged using fluorescence
 188 microscopy. We found that larger NPs were unable to enter
 189 the fixed cells, as they all remained at the cell surface even after
 190 24 h of incubation with NPs (Figure 2B). In sharp contrast,
 191 smaller NPs showed intracellular fluorescence already after 5
 192 min of incubation and then a strong intracellular signal after 24 h
 193 (Figure 2D). Thus, we could conclude that NPs of small size are
 194 required for the design of the FISH probe, which is in line with
 195 the earlier report based on QDs.⁶⁵ Our earlier works on live cells
 196 also showed that small size (<23 nm) was essential for free
 197 diffusion of NPs inside the cytosol.⁸⁰ 198

Then, we tested whether the hybridization with the poly(A)
 199 tails is specific. We replaced T20 DNA with A20 DNA, which is
 200 not expected to hybridize with the poly(A) targets. However,
 201 microscopy experiments showed that the intracellular signal for
 202 these NPs remained high, indicating strong nonspecific 203

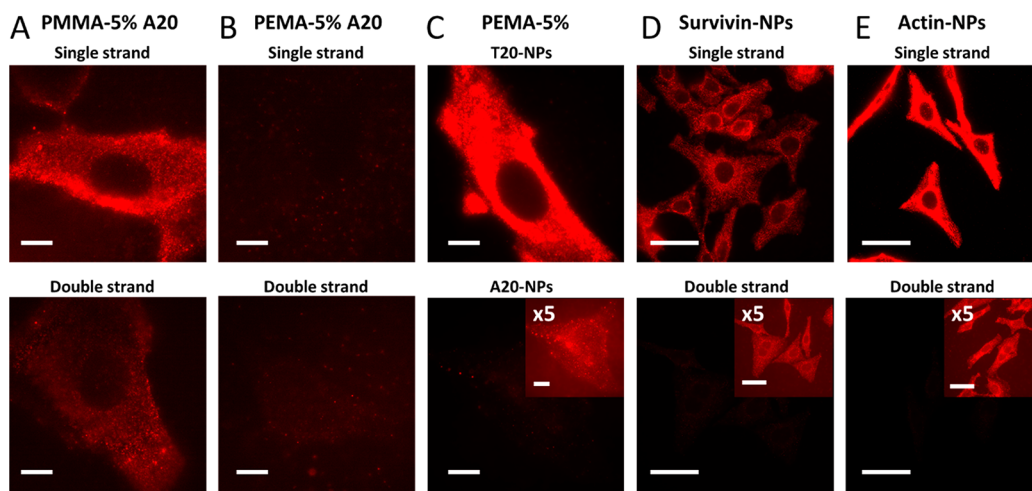


Figure 3. Effect of polymer nature and different grafted DNA sequences. (A, B) Fluorescence images of fixed HeLa cells incubated with PMMA-based NPs (A) and PEMA-based NPs (B) of ~ 20 nm core size, functionalized with A20. Both single-stranded and double-stranded (annealed with T20) DNA NPs were tested (30 min incubation with cells). TIRF mode was used on fixed HeLa cells without washing. (C) Comparison of TIRF fluorescence images of PEMA-based NPs functionalized with T20 (upper panel) and A20 (lower panel) recorded at identical conditions (inset shows an image where the signal was amplified 5-fold for visibility of the cell). Cells were incubated during 1 h with NPs, then washed two times with 0.1% BSA/PBS. Scale bar: 10 μm . (D, E) Epi-fluorescence microscopy of fixed HeLa cells incubated for 1 h with DNA-NPs targeting survivin and β -actin (the same washing protocol as in C). Images for single-stranded (upper panels) and double-stranded (annealed with complementary strands) DNA-NPs are shown. Scale bar: 50 μm . PBS buffer with 50 mg/L Tween 80 was systematically used for incubation and imaging (A–E).

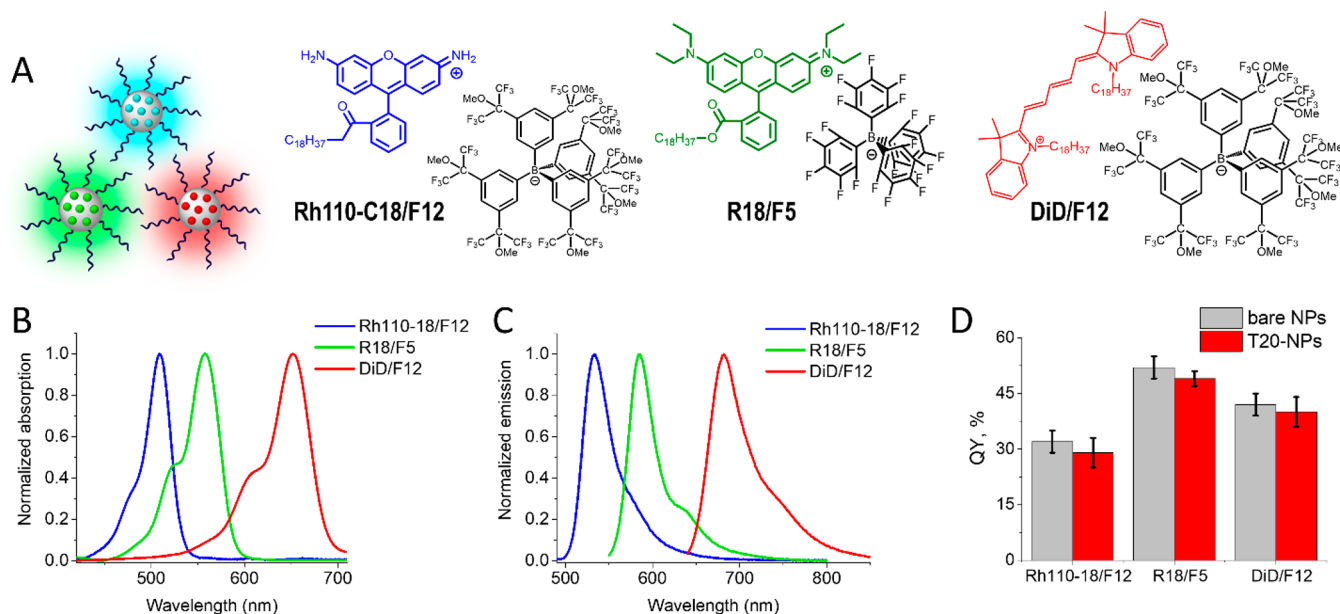


Figure 4. FISH-NPs of three different colors. (A) Dye salts with bulky counterions used for encapsulation into polymeric NPs. (B) Absorption and (C) fluorescence spectra of DNA-NP loading three different dye salts. (D) Fluorescence quantum yields of bare NPs and DNA-NPs (T20 oligonucleotide). Dye loading (weight % ratio with respect to the polymer) was 30 wt %. Error bars are standard deviation ($n \geq 3$).

204 interactions of NPs inside the cells (Figure 3A). We further
 205 annealed the A20-functionalized NPs with T20 DNA to obtain
 206 double-stranded oligonucleotides at the NP surface. In this case,
 207 the intracellular signal decreased (Figures 3A and S1), but still
 208 remained significant, confirming the nonspecific interactions of
 209 NPs with the cells, independent from the DNA/RNA
 210 hybridization. Therefore, we formulated small NPs based on
 211 another polymer, PEMA bearing 5% charged groups (PEMA-
 212 MA-5%), which was previously shown to yield ~ 20 nm
 213 ultrabright NPs.⁵¹ Importantly, the cell experiments revealed
 214 practically no signal for A20-functionalized PEMA-based NPs

(Figures 3B and S1). A similar low intracellular signal was 215
 observed for the NPs bearing A20 annealed with T20 DNA. 216
 Then, we directly compared PEMA-based NPs functionalized 217
 with A20 DNA (A20-NPs) and T20 DNA (T20-NPs). A strong 218
 intracellular signal was observed in the case of T20-NPs, while 219
 the signal from A20-NPs was very weak and could only be 220
 detected when the signal in the image was multiplied 5-fold 221
 (Figures 3C and S1). Thus, the use of PEMA-based NPs 222
 dramatically decreased nonspecific interactions, allowing direct 223
 detection of T20-NPs specifically hybridized with poly(A) 224
 targets inside the cells. It could be related to the narrower size 225

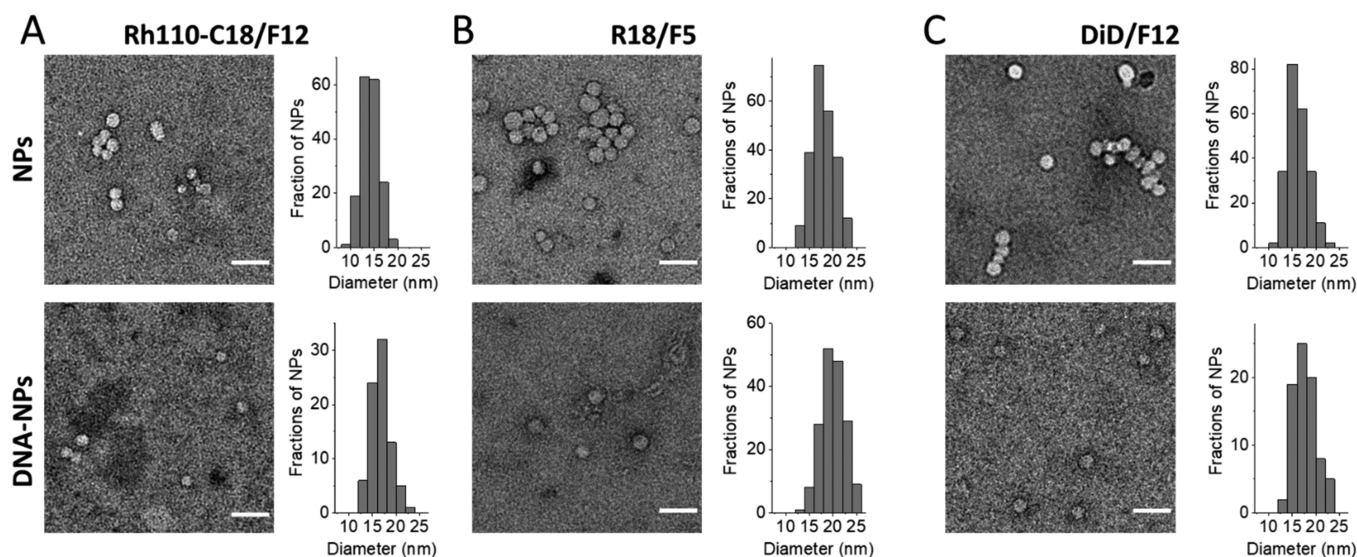


Figure 5. TEM characterization of DNA-NPs of different color functionalized with T20 oligonucleotides. TEM images of DNA-NPs loaded at 30 wt % with Rh110-18/F12 (A), R18/R5-TPB (B), and DiD/F12 (C) and corresponding size distribution histograms at the right (at least 200 NPs were analyzed per condition). Upper panels correspond to bare NPs, while lower panels correspond to DNA-NPs.

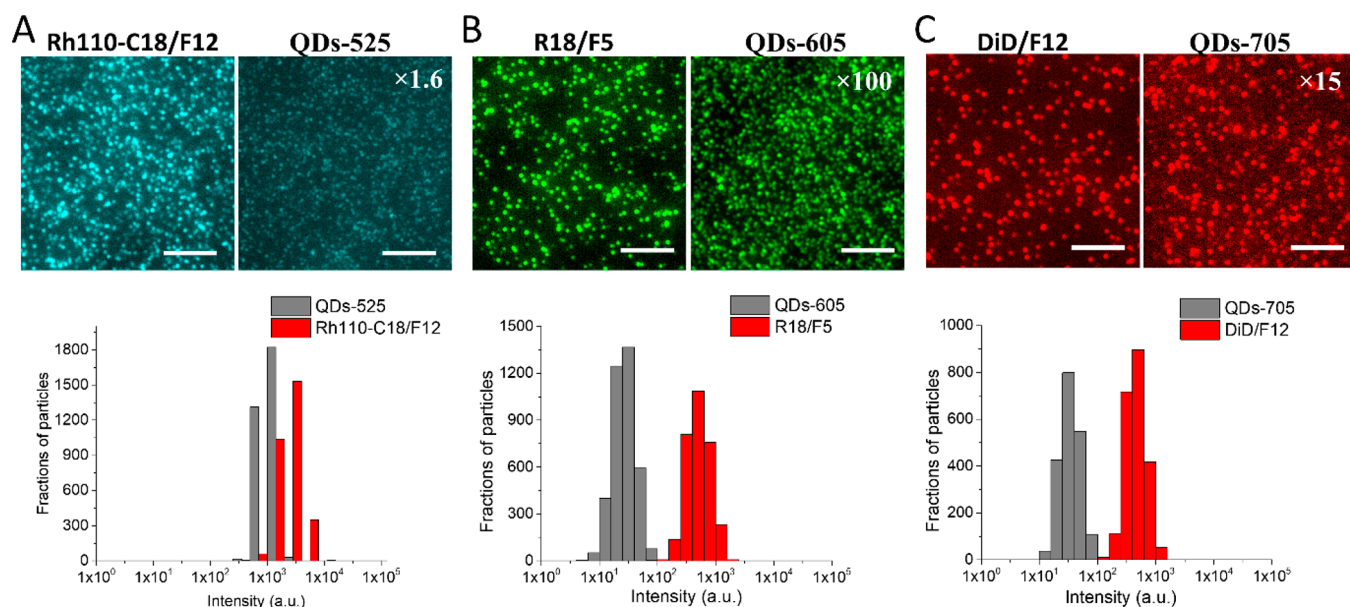


Figure 6. Single-particle characterization of DNA-NPs bearing T20 oligonucleotide in comparison to corresponding QDs on a glass surface using epi-fluorescence microscopy. Upper panels: Fluorescence images of DNA-NPs loaded at 30 wt % with Rh110-C18/F12 vs QDs-525 (A), R18/R5-TPB vs QDs-605 (B), and DiD/F12 vs QDs-705. The signal in QDs was multiplied 1.6- (A) 100- (B), and 15-fold (C) by a corresponding increase in the source power for better comparison with brighter DNA-NPs. Scale bar: 5 μ m. Lower panels: Corresponding intensity distribution histograms for DNA-NPs vs QDs.

226 distribution of these PEMA-based NPs (see below) compared to
 227 PMMA NPs. The second reason could be the more hydrophobic
 228 nature of PEMA compared to PMMA (ethyl vs methyl group),
 229 which can provide better stability to DNA-NPs, where the core
 230 is formed essentially due to hydrophobic collapse of the
 231 polymer. It should be added that the small size of PEMA-based
 232 NPs should limit the number of grafted oligonucleotides per
 233 particle to ~ 80 , according to our earlier studies on analogous
 234 DNA-NPs,⁵¹ which is important to minimize the off-target
 235 nonspecific interactions.

236 Then, we functionalized PEMA-based NPs with capture DNA
 237 sequences complementary to survivin and β -actin mRNA and
 238 tested them in cells. Both nanoprobe showed significant

intracellular signal inside the cells (Figures 3D,E and S2), which
 239 was significantly higher in the case of β -actin (see below). To
 240 verify the contribution of nonspecific interactions, we annealed
 241 our DNA-NPs with complementary short oligonucleotides in
 242 solution to block their capacity to hybridize with corresponding
 243 intracellular mRNA targets. Importantly, the intracellular signal
 244 decreased drastically for the double-stranded nanoprobe, so
 245 that 5-fold multiplication of the signal was required to observe
 246 some cell fluorescence (Figures 3D,E and S2). These first
 247 experiments showed that we could observe sequence-specific
 248 hybridization of our DNA-NPs with the intracellular mRNA
 249 targets. It should be noted that in all these images the nucleus 250

251 remained dark, indicating that NPs could not penetrate through
252 the nuclear envelope.

253 **DNA-NPs of Different Color.** Next, we prepared NPs of
254 three different colors in order to perform multicolor detection of
255 target mRNA. In addition to red-emitting R18/F5, we selected a
256 green rhodamine 110 derivative with an octadecyl chain
257 (Rh110-C18)⁸³ and far-red cyanine DiD (Figure 4). As a
258 counterion for these two dyes, we used the bulkiest available
259 counterion F12, which was shown previously to ensure the
260 highest fluorescence quantum yields (QYs) for the NPs.^{81,83} We
261 formulated bare NPs loaded with corresponding dyes and
262 checked the QYs at different dye loading. For all three dyes, QYs
263 decreased with an increase in the high loading (Table S1),
264 indicating some effect of dye self-quenching. On the basis of
265 these data, we could choose optimal high loading, where QYs
266 remained significantly high: 30 wt % for all three dye salts, with
267 quantum yields of 52%, 34%, and 42% for R18/F5, R110-C18/
268 F12, and DiD/F12. The size of the obtained bare NPs at 30 wt %
269 dye loading remained small according to dynamic light
270 scattering (DLS) (~17 nm) and TEM (14–18 nm, Table S2).
271 TEM imaging confirmed the spherical shape of bare NPs
272 (Figure 5). Then, we functionalized them with A20 or T20,
273 using the same protocol based on the SPAAC reaction. The QY
274 values did not change after functionalization and thus remained
275 relatively high. The absorption and fluorescence spectra of
276 DNA-NPs showed well-defined and well-separated bands
277 (Figure 4), typical for the molecular forms of these three dyes.
278 These bands match well common optical settings of the
279 microscope in the green, red, and far-red channels. According to
280 the TEM of DNA-NPs, the size of the spherically shaped
281 particles did not significantly change, since only a ~2 nm
282 increase was observed after functionalization (Figure 5, Table
283 S2). It is important to note the relatively narrow size distribution
284 of all these DNA-NPs, so that all detected NPs were
285 systematically <25 nm. This is a key difference with PMMA-
286 based NPs, where for similar particle size, NPs > 30 nm were still
287 observed (Figure 2C). This narrower size distribution could
288 explain why PEMA-based NPs showed much less nonspecific
289 interactions (or NP trapping) inside the cells (see above, Figure
290 3). On the other hand, DLS data suggested that after DNA
291 functionalization, the particle size increased by 6–7 nm (Table
292 S2), which corresponds to the lengths of two 20mer strands
293 grafted to the NP surface. In contrast to TEM, DLS records the
294 hydrodynamic diameter that takes into account the relatively
295 thick hydration shell formed by grafted nucleic acids.

296 Then, we characterized the obtained DNA-NPs at the single-
297 particle level using wide-field fluorescence microscopy. For each
298 color of NPs, we made a comparison with corresponding QDs
299 characterized by similar emission wavelength. All studied DNA-
300 NPs, which appeared as dots in the microscopy images, were
301 significantly brighter than corresponding QDs (Figure 6).
302 Quantitative analysis of the single-particle brightness revealed
303 that green, red, and far-red DNA-NPs were 2.3 ± 0.8 -, 97 ± 6 -,
304 and 16 ± 2 -fold brighter than corresponding QDs (Figure 6).
305 These differences correspond to the theoretical brightness (B)
306 of our NPs, which can be expressed as $B = N \times \epsilon \times QY/100$,
307 where N is the number of dyes per NP, ϵ is the absorption
308 coefficient ($M^{-1} \text{ cm}^{-1}$) at the excitation wavelength used, and
309 QY is the fluorescence quantum yield (%) of the dye inside the
310 NP. Taking the average NP size of bare NPs loaded with Rh110-
311 18/F12, R18/R5-TPB, and DiD/F12 NPs of 14, 18, and 16 nm,
312 respectively, according to TEM, and 30 wt % loading of the dyes
313 vs polymer (i.e., 23% vs total particle mass), the corresponding

314 estimated N is 85, 308, and 113. Then, the estimated single-
315 particle brightness is 6.9×10^5 , 1.8×10^7 , and $9.7 \times 10^6 M^{-1} \times$
316 cm^{-1} for Rh110-18/F12, R18/R5-TPB, and DiD/F12 NPs. For
317 QDs-525, QDs-605, and QDs-705, the measured QY values
318 were 77%, 52%, and 49%, respectively. Therefore, their
319 corresponding estimated brightness was 1.3×10^5 , 3.0×10^5 ,
320 and $4.4 \times 10^5 M^{-1} \text{ cm}^{-1}$ for excitation at 470, 550, and 640 nm,
321 respectively. Thus, theoretically, Rh110-18/F12, R18/R5-TPB,
322 and DiD/F12 should be 5.3-, 60-, and 22-fold brighter than
323 QDs-525, QDs-605, and QDs-705, respectively, which is close
324 to the obtained experimental values. We should note that these
325 differences would be smaller if QDs were excited at the violet
326 region, where their absorption coefficient is higher. The green
327 DNA-NPs were significantly less bright than the other two
328 DNA-NPs because of a lower absorption coefficient at the
329 excitation wavelength used (470 nm of LED), lower QY of this
330 dye, and less optimal emission filter settings. Overall, we
331 obtained DNA-NPs of similar small size and high brightness,
332 which can be used for multicolor RNA-FISH experiments.

333 **Multicolor Detection of mRNA.** We functionalized NPs of
334 three different colors with three capture sequences targeting
335 poly(A), β -actin, and survivin fragments of mRNA. After
336 incubation of DNA-NPs with fixed and permeabilized HeLa
337 cells, we observed corresponding staining in each channel: green
338 for β -actin, red for survivin, and blue for poly(A) targets (Figure
339 7). Then, to verify that the binding is sequence dependent, we
340 annealed each nanoprobe with a corresponding complementary
341 DNA oligonucleotide and tested in cells. The obtained double-
342 stranded DNA-NPs showed practically no emission inside cells,
343 which confirmed low nonspecific interactions between NPs and
344 cells. To provide a more direct control for the sequence

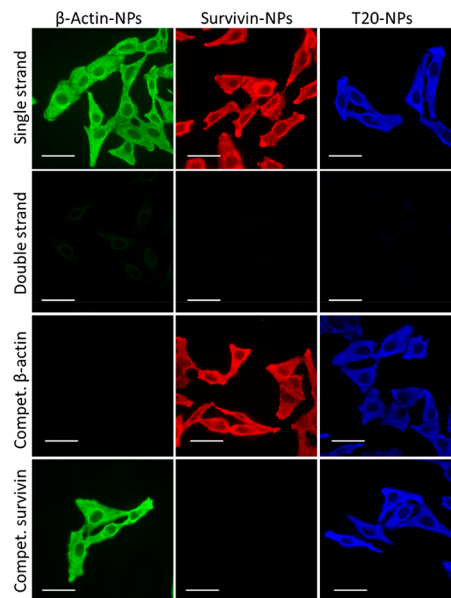


Figure 7. Validation of DNA-NPs for detection of intracellular mRNA targets in fixed HeLa cells. Single-stranded probes β -actin-NPs loaded with Rh110-C18/F12, survivin-NPs loaded with R18/F5, and A20-NPs loaded with DiD/F12 for β -actin, survivin, and poly(A) sequences of mRNA were compared to controls with double-stranded DNA-NPs (annealed with complementary sequences) and competitor oligonucleotides (100 nM) for corresponding β -actin and survivin sequences added 1 h before addition of DNA NPs. DNA-NPs concentration expressed in encapsulated dyes was 100 nM. Scale bar: 50 μm .

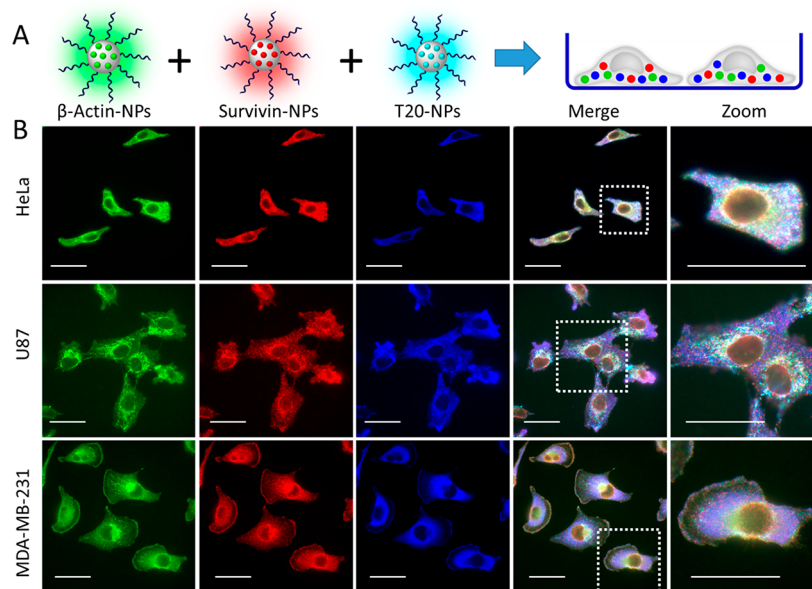


Figure 8. Multiplexed detection of mRNA sequences in fixed cells by AmpliFISH. (A) General principle and (B) corresponding epi-fluorescence images of three nanoprobe (the same as in Figure 7) β -actin-NPs (green), survivin-NPs (red), and T20-NPs (blue) in three cell lines: HeLa (upper row), U87 (middle row), and MDA-MB-231 (lower row). Merging of three channels and corresponding zoomed-in images of cells are also shown (last two columns). A mixture of the three different NPs at 100 nM (total dye concentration) was added to cells during 1 h, then washed two times before the observations. Scale bar: 50 μ m.

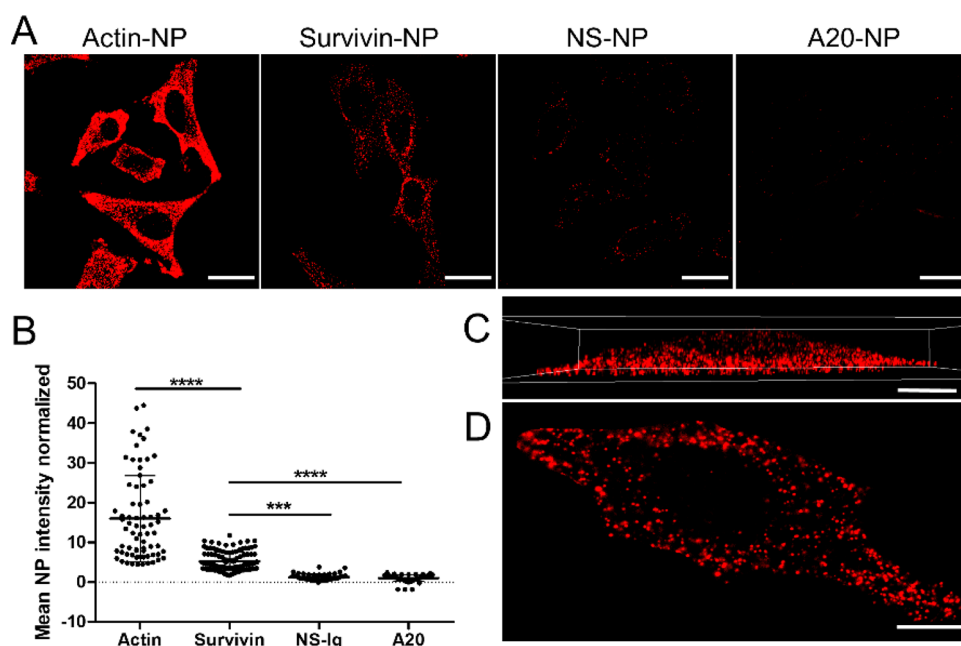


Figure 9. Imaging of HeLa cells using AmpliFISH with spinning-disk microscopy and quantification of the signal from mRNA targets. (A) Z-projection of multiple images of HeLa cells stained with different DNA-NPs. Scale bar: 30 μ m. (B) Quantification of total fluorescence intensity from DNA-NPs for four different target mRNA sequences. At least 100 cells were analyzed per condition in three independent measurements. *** $p < 0.001$, **** $p < 0.0001$. (C) 3D reconstruction of HeLa cells labeled with survivin-NPs. (D) Selected X–Y plane of the same cell as in (C) obtained by spinning-disk microscopy. Scale bar (C, D): 12 μ m.

345 specificity of our FISH probes, we treated the fixed and
 346 permeabilized cells with a competitive sequence complementary
 347 to the target (*i.e.*, identical to the capture sequence grafted to
 348 NPs), which is expected to block the site of binding of our
 349 nanoprobe. Importantly, the β -actin competitor turned off the
 350 intracellular signal from nanoprobe for β -actin, but did not
 351 influence those for survivin or poly(A) (Figure 7). By contrast, a
 352 competitive sequence encoding survivin blocked binding of

survivin nanoprobe, but did not affect those targeting actin or
 poly(A). These experiments showed that our NPs bind
 intracellular targets with sequence specificity for NPs of different
 color. We repeated these experiments for U87 (Figure S3) and
 MDA-MB-231 (Figure S4) cells and obtained similar results
 with excellent inhibition for both double-stranded version of
 NPs and the competitors for the β -actin and survivin mRNA
 targets. Thus, the approach works for multiple cell lines.

361 The next challenge was to image all three target sequences
362 simultaneously by exploiting three colors of NPs bearing
363 corresponding targeting oligonucleotides. To this end, fixed
364 and permeabilized HeLa, U87, and MDA-MB-231 cells were
365 incubated simultaneously with three NPs of different color and
366 further imaged using three channels of the microscope (Figure
367 8). Importantly, we could obtain signals for all three nanoprobe
368 within the same cell. Each cell showed a distinctive combination
369 of three colors distributed in space (Figure 8B). The green and
370 red colors, encoding β -actin-NPs and survivin-NPs, respectively,
371 did not really colocalize, which can be seen in the zoomed
372 images. This observation was confirmed by a Manders'
373 colocalization, giving relatively low values for β -actin-NPs in
374 survivin-NPs and *vice versa* for all three cell lines (with only one
375 exception for MDA-MB-231, Table S3). On the other hand,
376 each of them colocalized with the poly(A) target, which can be
377 seen from dominating magenta and cyan colors of the cells
378 (Figure 8B). Indeed, high Manders' colocalization coefficients
379 for β -actin-NPs in T20-NPs were observed, namely, 0.998,
380 0.998, and 0.935 for HeLa, U87, and MDA-MB-231,
381 respectively (Table S3). Similar high values were observed for
382 survivin. These observations can be explained by the fact that
383 both β -actin and survivin mRNAs are expected to have poly(A).
384 On the other hand, T20-NPs colocalized with much lower
385 Manders' coefficients with β -actin-NPs and survivin-NPs, which
386 is normal because there are many other mRNAs having a
387 poly(A) tail. In the perinuclear regions, all three colors appeared
388 colocalized, giving white pixels. The latter is probably because
389 too many particles of different color concentrated within areas
390 below the diffraction-limited resolution of the microscope,
391 which produced a colocalization effect, even if these NPs are not
392 bound to the same mRNA target. One could also notice that the
393 distribution of the three colors was slightly different for each
394 studied cell line. Indeed, HeLa cells showed a tendency to
395 redistribute colors in a rather homogeneous fashion, while the
396 U87 cells showed magenta colors (*i.e.*, survivin and poly(A))
397 localized at extremities of the cells (Figure 8B). In MDA-MB-
398 231 cells, the signals corresponding to β -actin and survivin
399 appeared in similar areas, including the cell edges, providing
400 characteristic yellow regions (Figure 8B). Thus, the combina-
401 tion of three nanoprobe reveals distinctive signatures of mRNA
402 distribution at the single-cell level for each cancer cell line.

403 **Quantification and Single-Particle Analysis.** We ex-
404 plored a possibility to quantify the observed fluorescence inside
405 the HeLa cells with different DNA-NPs loaded with the same
406 dye, R18/F5. In addition to β -actin, survivin, and A20, we
407 prepared nanoprobe functionalized with another noncoding
408 capture sequence (NP-NS) that does not correspond to any
409 mRNA in HeLa cells. Using spinning-disk fluorescence
410 microscopy, we recorded different planes of the cells and then
411 summed all stacks together. The resulting images could clearly
412 show the strong signal from β -actin-NPs, then a lower signal
413 from survivin-NPs and practically no signal from noncoding
414 sequence NS-NPs and A20-NPs (Figure 9A). Quantitative
415 analysis confirmed these observations, showing that the average
416 signal decreased in the following order: β -actin-NP \gg survivin-
417 NP \gg NS-NP > A20-NP (Figure 9B). RT-qPCR of the cells
418 revealed that mRNA of β -actin was much more abundant (Ct =
419 15.2) than that of survivin (Ct = 24.8), supporting our FISH
420 data. However, the differences revealed by RT-qPCR were
421 significantly larger than those observed by the AmpliFISH
422 method. Therefore, we consider that our approach at this step
423 remains semiquantitative. One should also note that NS-NPs

showed a bit higher signal than A20-NPs, which indicates that a
part of the signal here could originate from off-target
interactions of the noncoding sequence. Taking into account
that the presence of a competitive sequence can completely
block the binding of corresponding DNA-NPs, we can conclude
that nonspecific binding of NPs could be related to some off-
target hybridization with shorter nucleic acid sequences, which
is a common problem of the FISH technique.^{41,88} This could
explain why at the current state our method remains
semiquantitative.

The remaining question regarding our DNA-NPs in cells was
whether the observed spots correspond to individual NPs. In the
wide-field microscopy images (Figures 7 and 8), it was difficult
to identify single particles because of poor Z-resolution and
strong contribution of out-of-focus NPs to the final images.
Therefore, we used spinning-disk microscopy to record the Z-
stack of image planes of cells labeled with survivin-NPs and then
reconstructed 3D images. In the 3D image (Figure 9C, Video
S1) and the individual XY image plane (Figure 9D), one could
clearly see individual dots distributed all around the cells, except
the nucleus, where NPs cannot really penetrate. In addition, we
recorded videos from one focal plane of HeLa cells labeled with
actin-NPs using spinning-disk microscopy. We found that the
majority of bright dots (with the exception of some larger spots)
showed some signal fluctuation/blinking (Video S2). This
fluorescence intermittence is typical for individual acrylate-
based R18/F5-loaded NPs due to cooperative effects of dyes
inside the polymeric particle.⁷⁸ Therefore, we can conclude that
these dots correspond to single particles immobilized inside the
cells through interactions with the target.

Comparison with the Classical FISH Method. To
benchmark the performance of AmpliFISH, a commercial
FISH technique was used, employing locked nucleic acid (LNA)
probes (Qiagen). The LNA technology provides improved
discriminating capacity of FISH probes and thus improved
sensitivity and specificity to the RNA targets.⁸⁹ Two types of
LNA probes were tested: LNA T25 in order to target poly(A) of
mRNA and LNA β -actin, which groups together several
sequences targeting actin mRNA. These two types of probes
are coupled to digoxigenin (3'DIG) to allow indirect detection
of mRNA targets (primary antibody then secondary antibody
coupled to Alexa Fluor 488). The results obtained for these two
probes as well as the negative control (absence of probe) for the
U87 line are illustrated in Figure 10. On one hand, there is
indeed an absence of fluorescence signal for the negative control
without LNA probes, ruling out nonspecific interactions in the
cells. On the other hand, a fluorescence signal is obtained for the
LNA probes in the fixed and permeabilized U87MG cells, in the
cytosol and in the nucleus. Unlike DNA-NPs, these probes are
capable of detecting their target in the nucleus, owing to their
smaller size. However, the key difference was the obtained signal
with the commercial probes was 8 times lower compared to that
obtained with our green emission DNA-NPs loaded with
Rh110-18/F12. Taking into account that our red NPs loaded
with R18/F5 are 25 times brighter than the green ones (see
above), our AmpliFISH technique based on R18/F5 should
provide a 200-fold stronger signal compared to the LNA FISH
method. This drastic difference originates from the much higher
brightness of our NPs (80–300 dyes per NP) compared to the
fluorescently labeled antibodies. In addition, our technique is
much simpler and faster compared to the commercial FISH
composed of >20 steps before microscopy accompanied by
multiple washes between each step.

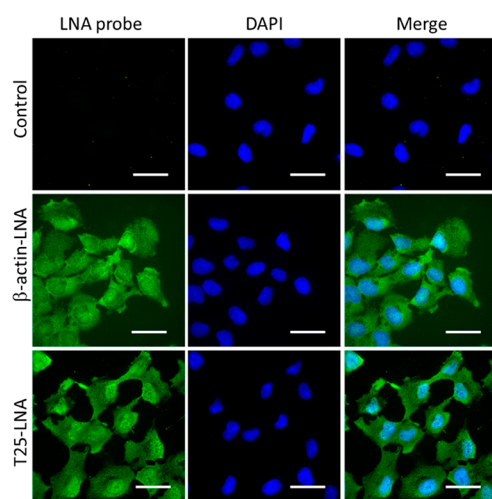


Figure 10. Commercial LNA probes at 25 nM for the detection of actin mRNA and poly(A) tails in U87 cells. Epi-fluorescence images of the FISH LNA probes and nuclei (DAPI) as well as the superposition (merge) of the two images (scale bar: 50 μm).

MATERIALS AND METHODS

525

Chemical Synthesis. Chemicals were purchased from either Sigma-Aldrich, Alfa Aesar, or ThermoFisher Scientific. NMR spectra were recorded at 20 $^{\circ}\text{C}$ on a Bruker Avance III 400 MHz spectrometer, and chemical shifts were reported as delta scale in ppm relative to CHCl_3 ($\delta = 7.26$ ppm) for ^1H NMR and CDCl_3 ($\delta = 77.16$ ppm) for ^{13}C NMR. Mass spectra were obtained using an Agilent Q-TOF 6520 mass spectrometer. Polymers PMMA-AspN3-1.6%, PMMA-AspN3-5%, and PEMA-AspN3 were synthesized as described previously^{51,52} Rhodamine B octadecyl ester trakis(pentafluorophenyl)borate (R18/F5) and DiD/F12 were synthesized by ion exchange and purified by column chromatography as described previously.^{77,81} Rhodamine 110 octadecyl ester (Rh110-C18/Cl) was synthesized by coupling of rhodamine 110 chloride and 1-octadecanol in the presence of sulfuric acid, followed by column chromatography purification as described elsewhere.⁹⁰ Rhodamine 110 octadecyl ester tetrakis[3,5-bis(1,1,1,3,3,3-hexafluoro-2-methoxy-2-propyl)phenyl]borate trihydrate (Rh110-C18/F12) was obtained by the ion exchange of obtained Rh110-C18/Cl with a sodium tetrakis[3,5-bis(1,1,1,3,3,3-hexafluoro-2-methoxy-2-propyl)phenyl]borate trihydrate (F12) followed by purification on preparative TLC using dichloromethane/methanol 95/5 as eluent.

Preparation of NPs. Sodium phosphate monobasic (>99.0%, Sigma-Aldrich) and sodium phosphate dibasic dihydrate (>99.0%, Sigma-Aldrich) were used to prepare 20 mM phosphate buffers. Sodium tetraborate decahydrate (>99.0%, Sigma-Aldrich) was used to prepare borate buffer. The final pH was adjusted with 0.1 M hydrochloric acid or 0.1 M sodium hydroxide. Milli-Q water (Millipore) was used in all experiments.

NP-PMMA-MA-1.6%. A 100 μL amount of the polymer solution in acetonitrile (2 mg mL^{-1} with 30 wt % of R18/F5 relative to the polymer) was added quickly using a micropipet to 900 μL of 20 mM phosphate buffer, pH 7.4, under shaking (Thermomixer comfort, Eppendorf, 1100 rpm). Then, the residues of acetonitrile were evaporated.

NP-PMMA-MA-5% and NP-PEMA-MA (Multicolor). A 50 μL amount of the polymer solution in acetonitrile (2 mg mL^{-1} containing Rh110-C18/F12 at 30 wt %, R18/F5 at 50 wt %, or DiD/F12 at 30 wt % relative to the polymer) was added quickly using a micropipet to 450 μL of 10 mM borate buffer, pH 9, at 21 $^{\circ}\text{C}$ under shaking (Thermomixer comfort, Eppendorf, 1100 rpm). While continuing mixing, 500 μL of 20 mM phosphate buffer, pH 6, was added. Then, the residues of acetonitrile were evaporated. The particle solution was then diluted 2-fold with the 20 mM phosphate buffer, pH 7.4.

General Protocol for Functionalization of NPs with DNA. Lyophilized single-strand DNA sequences were purchased from IBA GmbH, dissolved in Milli-Q water, aliquoted, and stored at -20 $^{\circ}\text{C}$ for further experiments. Aliquots of corresponding DNA-DBCO (concentration of 60 μM in the reaction mixture) were added to 200 μL of corresponding nanoparticles. The reaction was mixed and kept overnight at 40 $^{\circ}\text{C}$ without shaking protected from light. Then the reaction was cooled to room temperature. In the case of NPs with a double strand, to 100 μL of the reaction mixture an aliquot of DNA-target sequence in a 1:1 ratio with DNA-DBCO was added and the mixture was heated to 70 $^{\circ}\text{C}$ in a water bath for 3 min. To complete hybridization, the reaction was cooled to room temperature and kept in the dark for 2 h. Then, in the case of single-strand nanoparticles the mixture was diluted with 20 mM phosphate buffer to 4 mL. In the case of the double-strand nanoparticles, the mixture was diluted with 20 mM phosphate buffer containing 12 mM MgCl_2 and 30 mM NaCl to 4 mL. Both types of NPs were purified by centrifugation using centrifuge filters (Amicon, 0.5 mL, 100 kDa, Sigma-Aldrich) at 1000g at 20 $^{\circ}\text{C}$ for 2 min. The procedure of centrifugation was repeated five times to remove the nonreacted oligonucleotides using the corresponding buffer. The obtained functionalized DNA-NPs were kept in the dark at 4 $^{\circ}\text{C}$.

The oligonucleotide sequences used in this study are shown below: SurC-DBCO, 5'-CCC AGC CTT CCA GCT CCT TGA-(DBCO)-3'

CONCLUSIONS

The development of simple and direct methods for the detection of mRNA inside the cells, which could accelerate biological and biomedical research and clinical diagnostics, remains a high challenge. To address this problem, we propose an amplified FISH methodology (AmpliFISH): ultrabright DNA-functionalized polymeric NPs are specially designed to penetrate cells and detect their intracellular mRNA targets. We synthesized NPs of different sizes and polymeric matrices. We found that the size of NPs below 20 nm is crucial for penetration and mRNA targeting in the fixed and permeabilized cells. Moreover, the nature of the polymer can drastically influence nonspecific interactions, which allowed us to select polymeric NPs showing the highest specificity. The obtained DNA-NPs enable sequence-specific detection and imaging of mRNA encoding β -actin, survivin, and its poly(A) tail, based on a very simple protocol of cell preparation and short incubation with NPs. Moreover, a combination of three different colors enables simultaneous detection of three mRNA targets within the same cell, showing feasibility of simple multiplexing single-cell transcriptome analysis. Importantly, each cancer cell line displayed a characteristic intracellular distribution of the three mRNA sequences, like a cell fingerprint. Moreover, the method allows semiquantitative analysis of mRNA in cells, although an additional dedicated study will be required to make it a truly quantitative single-cell mRNA detection method. Single-particle video microscopy confirmed that the majority of the intracellular signal corresponds to individual particles, which should enable mRNA detection with single-molecule sensitivity. Comparison with the commercial FISH technique based on LNA oligonucleotides showed that our method has multiple advantages: (i) it provides 8–200-fold stronger signal (dependent on the NP color); (ii) it is based on three steps vs ~ 20 steps in the commercial technique as well as much shorter time. Thus, the developed AmpliFISH approach has the potential to significantly improve the current methods of transcriptomic analysis at the single-cell level, which is important for both biological research and clinical diagnostics.

594 SurC-Target, 5'-CAA GGA GCT GGA AGG CTG GG-3'
595 SurC-Competitive, 5'-CCC AGC CTT CCA GCT CCT TGA-3'
596 Actin-DBCO, 5'-CTG ACC CAT GCC CAC CAT CA-(DBCO)-3'
597 Actin-Target, 5'-TGA TGG TGG GCA TGG GTC AG-3'
598 Actin-Competitive, 5'-CTG ACC CAT GCC CAC CAT CA-3'
599 T20-DBCO, 5'-TT TTT TTT TTT TTT TT-(DBCO)-3'
600 T20, 5'-TT TTT TTT TTT TTT TT-3'
601 A20-DBCO, 5'-AAA AAA AAA AAA AAA AA-(DBCO)-3'

602 **Characterization of NPs.** Dynamic light scattering (DLS) measurements were performed on a Zetasizer Nano ZSP (Malvern Instruments S.A.). The Zetasizer software provided with standard cumulates and size distribution by volume analysis was used to characterize nanoparticles by DLS. For the data analysis, the following parameters were used: for the solvent (water), temperature 25 °C, refractive index RI 1.33, and viscosity 0.8872 cP. Nanoparticles were assumed to be all homogeneous and spherical in shape. Absorption spectra were recorded on a Cary 5000 scan UV-visible spectrophotometer (Varian). Excitation, emission spectra, and anisotropy were recorded on a F55 spectrofluorometer (Edinburg Instruments). For standard recording of fluorescence spectra, the excitation wavelength was set to 470 nm (Rh110-C18/F12), 530 nm (R18/F5), and 640 nm (DiD/F12). The fluorescence spectra were corrected for detector response and lamp fluctuations. Quantum yields of NPs and QDots were calculated using fluorescein in 10 mM NaOH (QY = 1.0), rhodamine 101 in methanol (QY = 1.0),⁹¹ and DiD in methanol (QY = 0.33)⁹² as the corresponding references.

620 **Transmission Electron Microscopy.** Carbon-coated copper–rhodium electron microscopy grids with a 300 mesh (Euromedex, France) were surface treated with a glow discharge in amylamine atmosphere (0.45 mbar, 5–5.3 mA, 25 s) in an Elmo glow discharge system (Cordouan Technologies, France). Then, 5 μ L of the solution of NPs was deposited onto the grids and left for 2 min. The grids were then treated for 1 min with a 2% uranyl acetate solution for staining. They were observed with the Tecnai F20 electron microscope, equipped with a FEG operated at 200 keV. Areas covered with nanoparticles of interest were recorded at 29000 \times magnifications on a GATAN CCD 2K*2K “US10001” camera. Image analysis was performed using the Fiji software.

632 **Single-Particle Fluorescence Microscopy.** Immobilization of DNA-NPs and QDots was done as follows. The LabTek chamber (borosilicate cover glass, eight wells, ThermoFisher Scientific) was washed three times with PBS followed by incubation with 200 μ L of bovine serum albumin (BSA)–biotin (Sigma-Aldrich) 0.5 mg mL⁻¹ in PBS for 5 min. Then, the BSA–biotin solution was removed, and the chamber was washed three times with 500 μ L of PBS. In the case of nanoparticle immobilization, the chamber was incubated with 200 μ L of neutravidin (ThermoFisher Scientific) solution (0.5 mg mL⁻¹ in PBS) for 5 min and washed three times with 500 μ L of PBS. Then the chamber was incubated with 200 μ L of a 1 μ M solution of A20-biotin in PBS for 5 min and washed one time with PBS and two times with 20 mM phosphate buffer. Then the nanoprobe solution was deposited with proper concentration to achieve the desired density and incubated for 1 h at room temperature in the dark. Before measurements the chamber was washed two times with 20 mM phosphate buffer and covered with 200 μ L of the same buffer. In the case of QDot immobilization, QDot525 streptavidin conjugate, QDot605 streptavidin conjugate, and QDot705 streptavidin conjugate (ThermoFisher Scientific) were diluted to 10 pM final concentration in PBS, and 300 μ L was added to the chamber. After 1 h of incubation, the chamber was washed three times with 500 μ L and filled with 200 μ L of PBS.

654 Single-particle microscopy measurements were performed in the epi-fluorescence mode using a Nikon Ti-E inverted microscope with a 100 \times objective (Apo TIRF, oil, NA 1.49, Nikon). The excitation was provided by light-emitting diodes (SpectraX, Lumencor) with the following wavelength and power density: 470 nm at 14 and 23 W cm⁻² for Rh110-C18/F12 NPs and QDot525, respectively; 550 nm at 0.24 and 24 W cm⁻² for R18/F5 NPs and QDot605, respectively, and 640 nm at 1.1 and 17 W cm⁻² for DiD/F12 NPs and QDot705. The exposure time was set to 400 ms per image frame. The fluorescence signal was recorded with a Hamamatsu Orca Flash 4 camera.

Single-particle analysis was performed using the Fiji software. 664 Particle locations were detected through a Fiji routine applied to a 665 projection (maximum intensity) of all obtained frames per experiment. 666 After the automatic background subtraction, the mean intensities of 667 circular regions of interest with a diameter of 8 pixels around the found 668 particle locations were then measured. At least three image sequences 669 (245 pixel \times 245 pixel) per condition with, on average, 1000–2000 670 particles per sample were analyzed. 671

672 **Cell Culture.** HeLa cells (ATCC CCL-2) were grown in Dulbecco's 673 modified Eagle's medium low glucose (DMEM, Gibco), supplemented 674 with 10% fetal bovine serum (FBS, Dutscher), 1% L-glutamine (Lonza), 675 and 1% penicillin–streptomycin (Lonza). The human glioblastoma cell 676 line U87 (ATCC) was maintained in minimum essential medium 677 (MEM, Gibco) supplemented with 10% FBS, 1% L-glutamine, 1% 678 sodium pyruvate (Lonza), and 1% nonessential amino acid (Lonza). 679 The human breast cancer cell line MDA-MB-231 (ATCC) was grown 680 in MEM (Gibco) supplemented with 10% FBS and 1% ultraglutamine 681 (Lonza). All cell lines were maintained at 37 °C in a humidified 682 atmosphere containing 5% CO₂. For the different experiments, cells 683 were seeded in eight-well LabTek plates (ThermoFisher) at 8000 cells/ 684 well overnight.

685 **Cell Fixation and Permeabilization.** For the fixation step, a 686 standard protocol of immunofluorescence was applied. First, cells were 687 washed one time with Dulbecco's phosphate-buffered saline (DPBS, 688 Lonza) and incubated with 4% PFA during 12 min at 37 °C. Cells were 689 then washed two times with DPBS and incubated 1 min at RT with 690 0.1% Triton X-100. Then, cells were washed two times with DPBS and 691 incubated in 3% BSA/DPBS (Sigma) for 1 h 30 min at RT. The final 692 step was to remove the 3% BSA/DPBS solution and incubate cells in 693 DPBS. The fixed cells can be used just after fixation or can be kept at 4 694 °C until their utilization.

695 **In Situ Hybridization with DNA-NPs.** Independently of the DNA 696 sequence used, DNA-NPs were first diluted to 100 nM concentration in 697 0.1% BSA/DPBS. Then, DPBS from the fixed permeabilized cells was 698 removed and the diluted DNA-NPs were added to the cells for 1 h at RT 699 or 37 °C. Then, cells were washed two times with 0.1% BSA/DPBS to 700 remove the DNA-NPs that were not hybridized with the RNA target 701 and were observed by the microscope in 0.1% BSA/DPBS.

702 In the case of competition experiments, cells were preincubated for 1 703 h at RT with a complementary DNA sequence to actin or survivin 704 mRNA target at 100 nM diluted in 0.1% BSA/DPBS. Without any 705 washing step, NPs were directly added on cells, followed by the above- 706 described protocol.

707 **Cell Imaging.** At the beginning of the study, cells and NPs were 708 observed at TIRF mode using a Nikon Ti-E inverted microscope with a 709 100 \times objective (Apo TIRF, oil, NA 1.49, Nikon). The excitation 710 wavelength was 550 nm with a power density of 26 W cm⁻²; emission 711 was recorded with a 600/50 nm band-pass filter. Then, images were 712 acquired in epi-fluorescence mode with a Nikon Ti-E inverted 713 microscope, with a 60 \times oil objective (NA 1.4, Nikon) and a 714 Hamamatsu Orca Flash 4 sCMOS camera. The excitation was provided 715 by light-emitting diodes (LED, SpectraX, Lumencor). Acquisition 716 settings were as follows: for Rh110-C18/F12 NPs (ex. 470 nm; 717 emission: 531/40 nm band-pass filter) with an excitation power density 718 of 5 W cm⁻² and exposure time of 300 ms, for R18/F5 NPs (ex. 550 nm; 719 emission: 600/50 nm band-pass filter) with an excitation power density 720 of 3 W cm⁻² and exposure time of 200 ms, and for DiD/F12 NPs (ex. 721 638 nm; emission: 705/72 nm band-pass filter) with an excitation 722 power density of 1.3 W cm⁻² and exposure time of 200 ms. The images 723 were recorded using NIS Elements and then processed with ImageJ 724 software. Colocalization analysis was performed using Manders' 725 coefficient with the JACoP plugin in Fiji software. A threshold was 726 applied for each channel of all images (1685 to actin, 1613 to survivin, 727 and 1531 to T20).

728 Quantitative cellular imaging with R18/F5 NPs (Figure 9) was 729 performed using a Nikon Ti-E inverted microscope, equipped with a 730 CFI Plan Apo 60 \times oil (NA = 1.4) objective, X-Light spinning-disk 731 module (CREST Optics), and a Hamamatsu Orca Flash 4 sCMOS 732 camera with a 600/50 nm band-pass filter. The excitation in confocal 733 mode was provided by a 532 nm diode laser (OXXIUS). The exposure

734 time in confocal mode was set to 500 ms per image frame. All the images
735 were recorded using NIS Elements and then processed using Fiji
736 software. Background was removed in all images using a filter rolling
737 ball with a 20 pixels' radius and a sliding paraboloid shape. All images
738 are presented with the same brightness and contrast. Mean fluorescence
739 intensity was measured on the 3D stack for around 100 cells per
740 condition from three independent experiments. Statistical analysis was
741 done with the ANOVA algorithm.

742 **RT-qPCR.** Cell line selection was based on surviving mRNA
743 expression. Two days before RNA extraction, 10^6 cells were seeded in
744 100 mm Petri dishes. Total RNA was isolated using a miRNeasy mini
745 kit (Qiagen) following the protocol provided by the manufacturer. The
746 final volume of elution was 40 μ L. The quantity of total RNA was
747 determined using a Nanodrop (Thermo Scientific). RNA samples were
748 aliquoted and stored at -80 °C. Then, 1 μ g of RNA extracted was
749 transcribed into cDNA using miScript II reverse transcription kit
750 (Qiagen). mRNA expression was evaluated by relative quantitative RT-
751 qPCR analysis using the Fast SYBR Green Master Mix PCR kit
752 (Qiagen) and the StepOne Plus real time PCR system (Applied
753 Biosystem), according to the manufacturer's protocol. The primers
754 used were β -actin (RT²qPCR Primer Assay for Human ACTB,
755 NM_0011101, Qiagen) and BIRC5 (RT²qPCR Primer Assay for
756 HumanNM_001168, Qiagen). RT-PCR was carried out with human
757 RNA 18S (5'-TGTGGTGTGAGGAAAGCAG-3' and 5'-TCCAG
758 ACCATTGGCTAGGAC-3', Invitrogen) as internal reference. Target
759 cDNA expression was quantified using the comparative $\Delta\Delta$ Ct method
760 with 18S rRNA as an internal control.

761 **FISH with Commercial LNA Probe.** To compare our results with
762 commercial *in situ* hybridization, poly(T)25 and β -actin LNA probes
763 (Qiagen) were used coupled with DIG as described in the
764 manufacturer's protocol (Exiqon). The DIG proteins were detected
765 thanks to an indirect method, in order to amplify the signal with anti-
766 DIG primary antibody and secondary antibody coupled with
767 fluorochromes. Briefly, the first day, U87MG cells were seeded on 22
768 mm diameter coverslips deposited on six-well plates and allowed to rest
769 overnight. Then, cells were washed once with DPBS and fixed with 4%
770 PFA (Thermo Scientific)/5% acetic acid (Sigma) in DPBS for 15 min.
771 U87 cells were washed 2 \times 5 min in DPBS, treat with pepsin (Merck)
772 (0.1% in 10 mM HCl) for 1 min at 37 °C, and washed again two times
773 with water. At this step, cells were dehydrated through 70%, 90%, and
774 100% ethanol and allowed to dry a few seconds. Then, 25 μ L probes
775 diluted at 25 nM in hybridization buffer (50% deionized formamide
776 (Merck), 2 \times SSC (ThermoFisher), 50 mM sodium phosphate
777 (Merck), 10% dextran sulfate (Merck)) were put on a slide and
778 covered with the coverslips. The montage was heated at 80 °C for 75 s,
779 and the hybridization step was performed for 30 min in a humid
780 chamber at 55 °C for poly(T)25 probes and at 62 °C for β -actin probes.
781 Then, coverslips were washed with 2 \times SSC containing 0.1% Tween 20
782 and washed 3 \times 5 min with 0.1 \times SSC at 65 °C. Cells were dehydrated
783 through 70%, 90%, and 100% ethanol and allowed to dry a few seconds.
784 Finally, U87MG cells were incubated with 3% BSA/DPBS (Sigma) for
785 1 h 30 min at RT, followed by the anti-DIG grom mouse IgG primary
786 antibody (Sigma) at 1 μ g/mL in 3% BSA/DPBS overnight at 4 °C in a
787 humid chamber. The day after, cells were washed 3 \times 5 min in DPBS
788 and incubated with goat anti-mouse IgG secondary antibody coupled
789 with Alexa Fluor 488 nm (ThermoFisher) diluted at 1 μ g/mL and
790 DAPI (ThermoFisher) diluted at 5 μ g/mL for 45 min. After 3 \times 5 min
791 of washing with DPBS, cells were mounted on a microscope slide with
792 mounting medium (Dako) and allowed to dry in the dark overnight.
793 Finally, coverslips were observed with epi-fluorescence mode with a
794 Nikon Ti-E inverted microscope, with a 60 \times oil objective (numerical
795 aperture = 1.4) and a Hamamatsu Orca Flash 4 sCMOS camera. The
796 settings were as follows: DAPI (excitation 395 nm; emission 468–552
797 nm) with a power of 30% and exposure time of 200 ms and Alexa 488
798 nm (excitation 470 nm; emission 491–571 nm) with a power of 90%
799 and exposure time of 200 ms. The images were recorded using NIS
800 Elements and then processed with ImageJ software.

ASSOCIATED CONTENT

Supporting Information

The Supporting Information is available free of charge at
<https://pubs.acs.org/doi/10.1021/acsnano.1c09409>.

Additional characterization data, cellular images, and
colocalization analysis (PDF)

Video of an individual XY image plane (AVI)

Video of signal fluctuation/blinking (AVI)

AUTHOR INFORMATION

Corresponding Author

Andrey S. Klymchenko – Laboratoire de Bioimagerie et
Pathologies, UMR 7021 CNRS, Faculté de Pharmacie,
Université de Strasbourg, 67401 Illkirch, France;
orcid.org/0000-0002-2423-830X; Phone: +33 368 85 42
55; Email: andrey.klymchenko@unistra.fr

Authors

Sylvie Egloff – Laboratoire de Bioimagerie et Pathologies, UMR
7021 CNRS, Faculté de Pharmacie, Université de Strasbourg,
67401 Illkirch, France

Nina Melnychuk – Laboratoire de Bioimagerie et Pathologies,
UMR 7021 CNRS, Faculté de Pharmacie, Université de
Strasbourg, 67401 Illkirch, France

Elisabete Cruz Da Silva – Laboratoire de Bioimagerie et
Pathologies, UMR 7021 CNRS, Faculté de Pharmacie,
Université de Strasbourg, 67401 Illkirch, France;
orcid.org/0000-0003-3417-5661

Andreas Reisch – Laboratoire de Bioimagerie et Pathologies,
UMR 7021 CNRS, Faculté de Pharmacie, Université de
Strasbourg, 67401 Illkirch, France

Sophie Martin – Laboratoire de Bioimagerie et Pathologies,
UMR 7021 CNRS, Faculté de Pharmacie, Université de
Strasbourg, 67401 Illkirch, France

Complete contact information is available at:

<https://pubs.acs.org/10.1021/acsnano.1c09409>

Author Contributions

[§]S.E. and N.M. contributed equally to this work.

Notes

The authors declare the following competing financial
interest(s): Nina Melnychuk, Andreas Reisch, and Andrey S.
Klymchenko are inventors on a patent application related to this
technology (European patent application no. 18305253.9). The
remaining authors declare no competing interests.

ACKNOWLEDGMENTS

This work was supported by the European Research Council
ERC Consolidator Grant BrightSens 648525, ERC Proof of
Concept Grant AmpliFISH 899928, and SATT Conectus
Maturation Grant NanoAntenna. We thank Corinne Crucifix
from the FRISBI platform for her help with the electron
microscopy and Anne Runser for help with polymer synthesis.

REFERENCES

- Michellini, F.; Jalihal, A. P.; Francia, S.; Meers, C.; Neeb, Z. T.;
Rossiello, F.; Gioia, U.; Aguado, J.; Jones-Weinert, C.; Luke, B.;
Biamonti, G.; Nowacki, M.; Storici, F.; Carninci, P.; Walter, N. G.; di
Fagagna, F. D. From "Cellular" RNA to "Smart" RNA: Multiple Roles of
RNA in Genome Stability and Beyond. *Chem. Rev.* **2018**, *118*, 4365–
4403.

- 857 (2) Fatica, A.; Bozzoni, I. Long Non-Coding RNAs: New Players in
858 Cell Differentiation and Development. *Nat. Rev. Genet.* **2014**, *15*, 7–21.
- 859 (3) Xia, Y. Q.; Zhang, R. L.; Wang, Z. L.; Tian, J.; Chen, X. Y. Recent
860 Advances in High-Performance Fluorescent and Bioluminescent RNA
861 Imaging Probes. *Chem. Soc. Rev.* **2017**, *46*, 2824–2843.
- 862 (4) Dean, K. M.; Palmer, A. E. Advances in Fluorescence Labeling
863 Strategies for Dynamic Cellular Imaging. *Nat. Chem. Biol.* **2014**, *10*,
864 512–523.
- 865 (5) Tyagi, S. Imaging Intracellular RNA Distribution and Dynamics in
866 Living Cells. *Nat. Methods* **2009**, *6*, 331–338.
- 867 (6) Femino, A. M.; Fay, F. S.; Fogarty, K.; Singer, R. H. Visualization
868 of Single RNA Transcripts *in Situ*. *Science* **1998**, *280*, 585–590.
- 869 (7) Saliba, A.-E.; Westermann, A. J.; Gorski, S. A.; Vogel, J. Single-Cell
870 RNA-Seq: Advances and Future Challenges. *Nucleic Acids Res.* **2014**,
871 *42*, 8845–8860.
- 872 (8) Haque, A.; Engel, J.; Teichmann, S. A.; Lonnberg, T. A Practical
873 Guide to Single-Cell RNA-Sequencing for Biomedical Research and
874 Clinical Applications. *Genome Med.* **2017**, *9*, 75.
- 875 (9) Bertrand, E.; Chartrand, P.; Schaefer, M.; Shenoy, S. M.; Singer, R.
876 H.; Long, R. M. Localization of Ash1 mRNA Particles in Living Yeast.
877 *Mol. Cell* **1998**, *2*, 437–445.
- 878 (10) Paige, J. S.; Wu, K. Y.; Jaffrey, S. R. RNA Mimics of Green
879 Fluorescent Protein. *Science* **2011**, *333*, 642–646.
- 880 (11) Neubacher, S.; Hennig, S. RNA Structure and Cellular
881 Applications of Fluorescent Light-Up Aptamers. *Angew. Chem., Int.*
882 *Ed.* **2019**, *58*, 1266–1279.
- 883 (12) Filonov, G. S.; Moon, J. D.; Svensen, N.; Jaffrey, S. R. Broccoli:
884 Rapid Selection of an RNA Mimic of Green Fluorescent Protein by
885 Fluorescence-Based Selection and Directed Evolution. *J. Am. Chem.*
886 *Soc.* **2014**, *136*, 16299–16308.
- 887 (13) Bouhedda, F.; Fam, K. T.; Collot, M.; Autour, A.; Marzi, S.;
888 Klymchenko, A.; Ryckelynck, M. A Dimerization-Based Fluorogenic
889 Dye-Aptamer Module for RNA Imaging in Live Cells. *Nat. Chem. Biol.*
890 **2020**, *16*, 69–76.
- 891 (14) Sunbul, M.; Lackner, J.; Martin, A.; Englert, D.; Hacene, B.;
892 Grun, F.; Nienhaus, K.; Nienhaus, G. U.; Jaschke, A. Super-Resolution
893 RNA Imaging Using a Rhodamine-Binding Aptamer with Fast
894 Exchange Kinetics. *Nat. Biotechnol.* **2021**, *39*, 686–690.
- 895 (15) Gall, J. G.; Pardue, M. L. Formation and Detection of RNA-DNA
896 Hybrid Molecules in Cytological Preparations. *Proc. Natl. Acad. Sci. U.*
897 *S. A.* **1969**, *63*, 378–383.
- 898 (16) John, H. A.; Birnstiel, M. L.; Jones, K. W. RNA-DNA Hybrids at
899 the Cytological Level. *Nature* **1969**, *223*, 582–587.
- 900 (17) Bauman, J. G.; Wiegant, J.; Borst, P.; van Duijn, P. A New
901 Method for Fluorescence Microscopical Localization of Specific DNA
902 Sequences by *in Situ* Hybridization of Fluorochromelabelled RNA. *Exp.*
903 *Cell Res.* **1980**, *128*, 485–490.
- 904 (18) Langer-Safer, P. R.; Levine, M.; Ward, D. C. Immunological
905 Method for Mapping Genes on Drosophila Polytene Chromosomes.
906 *Proc. Natl. Acad. Sci. U. S. A.* **1982**, *79*, 4381–4385.
- 907 (19) Cui, C.; Shu, W.; Li, P. Fluorescence *in Situ* Hybridization: Cell-
908 Based Genetic Diagnostic and Research Applications. *Front. Cell Dev.*
909 *Biol.* **2016**, *4*, 89.
- 910 (20) Urbanek, M. O.; Krzyzosiak, W. J. RNA FISH for Detecting
911 Expanded Repeats in Human Diseases. *Methods* **2016**, *98*, 115–123.
- 912 (21) Raj, A.; Rinn, J. L. Illuminating Genomic Dark Matter with RNA
913 Imaging. *Cold Spring Harbor Perspect. Biol.* **2019**, *11*, a032094.
- 914 (22) Cui, C.; Shu, W.; Li, P. Fluorescence *in Situ* Hybridization: Cell-
915 Based Genetic Diagnostic and Research Applications. *Front. Cell Dev.*
916 *Biol.* **2016**, *4*, 89.
- 917 (23) Shaffer, S. M.; Joshi, R. P.; Chambers, B. S.; Sterken, D.; Biaisch,
918 A. G.; Gabrieli, D. J.; Li, Y.; Feemster, K. A.; Hensley, S. E.; Issadore, D.;
919 Raj, A. Multiplexed Detection of Viral Infections Using Rapid *in Situ*
920 RNA Analysis on a Chip. *Lab Chip* **2015**, *15*, 3170–3182.
- 921 (24) Kwon, S. Single-Molecule Fluorescence *in Situ* Hybridization:
922 Quantitative Imaging of Single RNA Molecules. *BMB Rep.* **2013**, *46*,
923 65–72.
- (25) Shaffer, S. M.; Wu, M.-T.; Levesque, M. J.; Raj, A. Turbo FISH: A
Method for Rapid Single Molecule RNA FISH. *PLoS One* **2013**, *8*,
e75120.
- (26) Femino, A.; Fay, F. S.; Fogarty, K.; Singer, R. H. Visualization of
Single RNA Transcripts *in Situ*. *Science* **1998**, *280*, 585–590.
- (27) Raj, A.; van den Bogaard, P.; Rifkin, S. A.; van Oudenaarden, A.;
Tyagi, S. Imaging Individual mRNA Molecules Using Multiple Singly
Labeled Probes. *Nat. Methods* **2008**, *5*, 877–879.
- (28) Jensen, E. Technical Review: *In Situ* Hybridization. *Anat. Rec.*
2014, *297*, 1349–1353.
- (29) Sinnamon, J. R.; Czaplinski, K. RNA Detection *in Situ* with FISH-
Stics. *RNA* **2014**, *20*, 260–266.
- (30) Xia, C.; Babcock, H. P.; Moffitt, J. R.; Zhuang, X. Multiplexed
Detection of RNA Using MerFISH and Branched DNA Amplification.
Sci. Rep. **2019**, *9*, 7721.
- (31) Wang, F.; Flanagan, J.; Su, N.; Wang, L. C.; Bui, S.; Nielson, A.;
Wu, X.; Vo, H. T.; Ma, X. J.; Luo, Y. RNAscope: A Novel *in Situ* RNA
Analysis Platform for Formalin-Fixed, Paraffin-Embedded Tissues. *J.*
Mol. Diagn. **2012**, *14*, 22–29.
- (32) Qing, Z. H.; Xu, J. Y.; Hu, J. L.; Zheng, J.; He, L.; Zou, Z.; Yang,
S.; Tan, W. H.; Yang, R. H. *In Situ* Amplification-Based Imaging of RNA
in Living Cells. *Angew. Chem., Int. Ed.* **2019**, *58*, 11574–11585.
- (33) Lizardi, P. M.; Huang, X.; Zhu, Z.; Bray-Ward, P.; Thomas, D. C.;
Ward, D. C. Mutation Detection and Single-Molecule Counting Using
Isothermal Rolling-Circle Amplification. *Nat. Genet.* **1998**, *19*, 225–
232.
- (34) Choi, H. M. T.; Chang, J. Y.; Trinh, L. A.; Padilla, J. E.; Fraser, S.
E.; Pierce, N. A. Programmable *in Situ* Amplification for Multiplexed
Imaging of mRNA Expression. *Nat. Biotechnol.* **2010**, *28*, 1208–1212.
- (35) Choi, H. M. T.; Beck, V. A.; Pierce, N. A. Next-Generation *in Situ*
Hybridization Chain Reaction: Higher Gain, Lower Cost, Greater
Durability. *ACS Nano* **2014**, *8*, 4284–4294.
- (36) Kishi, J. Y.; Lapan, S. W.; Believeau, B. J.; West, E. R.; Zhu, A.;
Sasaki, H. M.; Saka, S. K.; Wang, Y.; Cepko, C. L.; Yin, P. Saber
Amplifies FISH: Enhanced Multiplexed Imaging of RNA and DNA in
Cells and Tissues. *Nat. Methods* **2019**, *16*, 533–544.
- (37) Kishi, J. Y.; Schaus, T. E.; Gopalkrishnan, N.; Xuan, F.; Yin, P.
Programmable Autonomous Synthesis of Single-Stranded DNA. *Nat.*
Chem. **2018**, *10*, 155–164.
- (38) Rouhanifard, S. H.; Mellis, I. A.; Dunagin, M.; Bayatpour, S.;
Jiang, C. L.; Dardani, I.; Symmons, O.; Emert, B.; Torre, E.; Cote, A.;
Sullivan, A.; Stamatoyannopoulos, J. A.; Raj, A. ClampFISH Detects
Individual Nucleic Acid Molecules Using Click Chemistry-Based
Amplification. *Nat. Biotechnol.* **2019**, *37*, 84–89.
- (39) Orjalo, A.; Johansson, H. E.; Ruth, J. L. Stellaris Fluorescence *in*
Situ Hybridization (FISH) Probes: A Powerful Tool for mRNA
Detection. *Nat. Methods* **2011**, *8*, i–ii.
- (40) Narrandes, S.; Xu, W. Gene Expression Detection Assay for
Cancer Clinical Use. *J. Cancer* **2018**, *9*, 2249–2265.
- (41) Huber, D.; Voith von Voithenberg, L.; Kaigala, G. V. Fluorescence
in Situ Hybridization (FISH): History, Limitations and
What to Expect from Micro-Scale FISH? *Micro Nano Eng.* **2018**, *1*, 15–
24.
- (42) Chinen, A. B.; Guan, C. M.; Ferrer, J. R.; Barnaby, S. N.; Merkel,
T. J.; Mirkin, C. A. Nanoparticle Probes for the Detection of Cancer
Biomarkers, Cells, and Tissues by Fluorescence. *Chem. Rev.* **2015**, *115*,
10530–10574.
- (43) Wolfbeis, O. S. An Overview of Nanoparticles Commonly Used
in Fluorescent Bioimaging. *Chem. Soc. Rev.* **2015**, *44*, 4743–4768.
- (44) Howes, P. D.; Chandrawati, R.; Stevens, M. M. Colloidal
Nanoparticles as Advanced Biological Sensors. *Science* **2014**, *346*,
1247390.
- (45) Reisch, A.; Klymchenko, A. S. Fluorescent Polymer Nano-
particles Based on Dyes: Seeking Brighter Tools for Bioimaging. *Small*
2016, *12*, 1968–1992.
- (46) Algar, W. R.; Massey, M.; Rees, K.; Higgins, R.; Krause, K. D.;
Darwish, G. H.; Peveler, W. J.; Xiao, Z.; Tsai, H.-Y.; Gupta, R.; Lix, K.;
Tran, M. V.; Kim, H. Photoluminescent Nanoparticles for Chemical

- 992 and Biological Analysis and Imaging. *Chem. Rev.* **2021**, *121*, 9243–993 9358.
- 994 (47) Luan, J.; Seth, A.; Gupta, R.; Wang, Z.; Rath, P.; Cao, S.; 995 Gholami Derami, H.; Tang, R.; Xu, B.; Achilefu, S.; Morrissey, J. J.; 996 Singamaneni, S. Ultrabright Fluorescent Nanoscale Labels for the 997 Femtomolar Detection of Analytes with Standard Bioassays. *Nat.* 998 *Biomed. Eng.* **2020**, *4*, 518–530.
- 999 (48) Zhao, X. J.; Tapeç-Dytioco, R.; Tan, W. H. Ultrasensitive DNA 1000 Detection Using Highly Fluorescent Bioconjugated Nanoparticles. *J.* 1001 *Am. Chem. Soc.* **2003**, *125*, 11474–11475.
- 1002 (49) Hildebrandt, N.; Spillmann, C. M.; Algar, W. R.; Pons, T.; 1003 Stewart, M. H.; Oh, E.; Susumu, K.; Diaz, S. A.; Delehanty, J. B.; 1004 Medintz, I. L. Energy Transfer with Semiconductor Quantum Dot 1005 Bioconjugates: A Versatile Platform for Biosensing, Energy Harvesting, 1006 and Other Developing Applications. *Chem. Rev.* **2017**, *117*, 536–711.
- 1007 (50) Wu, W. B.; Bazan, G. C.; Liu, B. Conjugated-Polymer-Amplified 1008 Sensing, Imaging, and Therapy. *Chem.* **2017**, *2*, 760–790.
- 1009 (51) Melnychuk, N.; Egloff, S.; Runser, A.; Reisch, A.; Klymchenko, A. 1010 S. Light-Harvesting Nanoparticle Probes for FRET-Based Detection of 1011 Oligonucleotides with Single-Molecule Sensitivity. *Angew. Chem., Int.* 1012 *Ed.* **2020**, *59*, 6811–6818.
- 1013 (52) Melnychuk, N.; Klymchenko, A. S. DNA-Functionalized Dye- 1014 Loaded Polymeric Nanoparticles: Ultrabright FRET Platform for 1015 Amplified Detection of Nucleic Acids. *J. Am. Chem. Soc.* **2018**, *140*, 1016 10856–10865.
- 1017 (53) Ochmann, S. E.; Vietz, C.; Trofymchuk, K.; Acuna, G. P.; 1018 Lalkens, B.; Tinnefeld, P. Optical Nanoantenna for Single Molecule- 1019 Based Detection of Zika Virus Nucleic Acids without Molecular 1020 Multiplication. *Anal. Chem.* **2017**, *89*, 13000–13007.
- 1021 (54) Acuna, G. P.; Möller, F. M.; Holzmeister, P.; Beater, S.; Lalkens, 1022 B.; Tinnefeld, P. Fluorescence Enhancement at Docking Sites of DNA- 1023 Directed Self-Assembled Nanoantennas. *Science* **2012**, *338*, 506–510.
- 1024 (55) Vafaei, S.; Allabush, F.; Tabaei, S. R.; Male, L.; Dafforn, T. R.; 1025 Tucker, J. H. R.; Mendes, P. M. Förster Resonance Energy Transfer 1026 Nanoplatfrom Based on Recognition-Induced Fusion/Fission of DNA 1027 Mixed Micelles for Nucleic Acid Sensing. *ACS Nano* **2021**, *15*, 8517– 1028 8524.
- 1029 (56) He, D.; Wong, K.-W.; Dong, Z.; Li, H.-W. Recent Progress in 1030 Live Cell mRNA/MicroRNA Imaging Probes Based on Smart and 1031 Versatile Nanomaterials. *J. Mater. Chem. B* **2018**, *6*, 7773–7793.
- 1032 (57) Prigodich, A. E.; Seferos, D. S.; Massich, M. D.; Giljohann, D. A.; 1033 Lane, B. C.; Mirkin, C. A. Nano-Flares for mRNA Regulation and 1034 Detection. *ACS Nano* **2009**, *3*, 2147–2152.
- 1035 (58) Seferos, D. S.; Giljohann, D. A.; Hill, H. D.; Prigodich, A. E.; 1036 Mirkin, C. A. Nano-Flares: Probes for Transfection and mRNA 1037 Detection in Living Cells. *J. Am. Chem. Soc.* **2007**, *129*, 15477–15479.
- 1038 (59) Briley, W. E.; Bondy, M. H.; Randeria, P. S.; Dupper, T. J.; 1039 Mirkin, C. A. Quantification and Real-Time Tracking of RNA in Live 1040 Cells Using Sticky-Flares. *Proc. Natl. Acad. Sci. U. S. A.* **2015**, *112*, 1041 9591–9595.
- 1042 (60) Zhou, W. J.; Li, D. X.; Xiong, C. Y.; Yuan, R.; Xiang, Y. 1043 Multicolor-Encoded Reconfigurable DNA Nanostructures Enable 1044 Multiplexed Sensing of Intracellular MicroRNAs in Living Cells. *ACS* 1045 *Appl. Mater. Interfaces* **2016**, *8*, 13303–13308.
- 1046 (61) Li, N.; Wang, M. M.; Gao, X. N.; Yu, Z. Z.; Pan, W.; Wang, H. Y.; 1047 Tang, B. A DNA Tetrahedron Nanoprobe with Controlled Distance of 1048 Dyes for Multiple Detection in Living Cells and *in Vivo*. *Anal. Chem.* 1049 **2017**, *89*, 6670–6677.
- 1050 (62) Chandrasekaran, A. R.; Punnoose, J. A.; Zhou, L.; Dey, P.; Dey, 1051 B. K.; Halvorsen, K. DNA Nanotechnology Approaches for MicroRNA 1052 Detection and Diagnosis. *Nucleic Acids Res.* **2019**, *47*, 10489–10505.
- 1053 (63) He, L.; Lu, D.; Liang, H.; Xie, S.; Zhang, X.; Liu, Q.; Yuan, Q.; 1054 Tan, W. mRNA-Initiated, Three-Dimensional DNA Amplifier Able to 1055 Function inside Living Cells. *J. Am. Chem. Soc.* **2018**, *140*, 258–263.
- 1056 (64) Ma, Y.; Mao, G.; Huang, W.; Wu, G.; Yin, W.; Ji, X.; Deng, Z.; 1057 Cai, Z.; Zhang, X.-E.; He, Z.; Cui, Z. Quantum Dot Nanobeacons for 1058 Single RNA Labeling and Imaging. *J. Am. Chem. Soc.* **2019**, *141*, 1059 13454–13458.
- (65) Liu, Y.; Le, P.; Lim, S. J.; Ma, L.; Sarkar, S.; Han, Z. Y.; Murphy, S. 1060 J.; Kosari, F.; Vasmatzis, G.; Cheville, J. C.; Smith, A. M. Enhanced 1061 MRNA FISH with Compact Quantum Dots. *Nat. Commun.* **2018**, *9*, 1062 4461.
- (66) Qu, A. H.; Sun, M. Z.; Xu, L. G.; Hao, C. L.; Wu, X. L.; Xu, C. L.; 1063 Kotov, N. A.; Kuang, H. Quantitative Zeptomolar Imaging of MiRNA 1064 Cancer Markers with Nanoparticle Assemblies. *Proc. Natl. Acad. Sci. U.* 1065 *S. A.* **2019**, *116*, 3391–3400.
- (67) Pan, W.; Liu, B.; Gao, X. N.; Yu, Z. Z.; Liu, X. H.; Li, N.; Tang, B. 1066 A Graphene-Based Fluorescent Nanoprobe for Simultaneous Monitor- 1067 ing of MiRNA and MRNA in Living Cells. *Nanoscale* **2018**, *10*, 14264– 1068 14271.
- (68) Dong, H.; Dai, W.; Ju, H.; Lu, H.; Wang, S.; Xu, L.; Zhou, S. F.; 1069 Zhang, Y.; Zhang, X. Multifunctional Poly(L-Lactide)-Polyethylene 1070 Glycol-Grafted Graphene Quantum Dots for Intracellular MicroRNA 1071 Imaging and Combined Specific-Gene-Targeting Agents Delivery for 1072 Improved Therapeutics. *ACS Appl. Mater. Interfaces* **2015**, *7*, 11015– 1073 11023.
- (69) Kim, E.; Yang, J.; Park, J.; Kim, S.; Kim, N. H.; Yook, J. I.; Suh, J.- 1074 S.; Haam, S.; Huh, Y.-M. Consecutive Targetable Smart Nanoprobe for 1075 Molecular Recognition of Cytoplasmic MicroRNA in Metastatic Breast 1076 Cancer. *ACS Nano* **2012**, *6*, 8525–8535.
- (70) Wang, Y.; Wu, C.; Chen, T.; Sun, H.; Cansiz, S.; Zhang, L.; Cui, 1077 C.; Hou, W.; Wu, Y.; Wan, S.; Cai, R.; Liu, Y.; Sumerlin, B. S.; Zhang, 1078 X.; Tan, W. DNA Micelle Flares: A Study of the Basic Properties That 1079 Contribute to Enhanced Stability and Binding Affinity in Complex 1080 Biological Systems. *Chem. Sci.* **2016**, *7*, 6041–6049.
- (71) Dong, X.; Ong, S. Y.; Zhang, C.; Chen, W.; Du, S.; Xiao, Q.; Gao, 1081 L.; Yao, S. Q. Broad-Spectrum Polymeric Nanoquencher as an Efficient 1082 Fluorescence Sensing Platform for Biomolecular Detection. *ACS Sens.* 1083 **2021**, *6*, 3102–3111.
- (72) Lin, L.-S.; Cong, Z.-X.; Cao, J.-B.; Ke, K.-M.; Peng, Q.-L.; Gao, J.; 1084 Yang, H.-H.; Liu, G.; Chen, X. Multifunctional Fe₃O₄@Polydopamine 1085 Core-Shell Nanocomposites for Intracellular MRNA Detection and 1086 Imaging-Guided Photothermal Therapy. *ACS Nano* **2014**, *8*, 3876– 1087 3883.
- (73) Sahay, G.; Alakhova, D. Y.; Kabanov, A. V. Endocytosis of 1088 Nanomedicines. *J. Controlled Release* **2010**, *145*, 182–195.
- (74) Iversen, T. G.; Skotland, T.; Sandvig, K. Endocytosis and 1089 Intracellular Transport of Nanoparticles: Present Knowledge and Need 1090 for Future Studies. *Nano Today* **2011**, *6*, 176–185.
- (75) Patel, S.; Kim, J.; Herrera, M.; Mukherjee, A.; Kabanov, A. V.; 1091 Sahay, G. Brief Update on Endocytosis of Nanomedicines. *Adv. Drug* 1092 *Delivery Rev.* **2019**, *144*, 90–111.
- (76) Ong, S. Y.; Zhang, C.; Xiao, D.; Yao, S. Q. Recent Advances in 1093 Polymeric Nanoparticles for Enhanced Fluorescence and Photo- 1094 acoustic Imaging. *Angew. Chem., Int. Ed.* **2021**, *60*, 17797–17809.
- (77) Reisch, A.; Didier, P.; Richert, L.; Oncul, S.; Arntz, Y.; Mely, Y.; 1095 Klymchenko, A. S. Collective Fluorescence Switching of Counterion- 1096 Assembled Dyes in Polymer Nanoparticles. *Nat. Commun.* **2014**, *5*, 1097 4089.
- (78) Reisch, A.; Trofymchuk, K.; Runser, A.; Fleith, G.; Rawiso, M.; 1098 Klymchenko, A. S. Tailoring Fluorescence Brightness and Switching of 1099 Nanoparticles through Dye Organization in the Polymer Matrix. *ACS* 1100 *Appl. Mater. Interfaces* **2017**, *9*, 43030–43042.
- (79) Reisch, A.; Runser, A.; Arntz, Y.; Mely, Y.; Klymchenko, A. S. 1101 Charge-Controlled Nanoprecipitation as a Modular Approach to 1102 Ultrasmall Polymer Nanocarriers: Making Bright and Stable Nano- 1103 particles. *ACS Nano* **2015**, *9*, 5104–5116.
- (80) Reisch, A.; Heimburger, D.; Ernst, P.; Runser, A.; Didier, P.; 1104 Dujardin, D.; Klymchenko, A. S. Protein-Sized Dye-Loaded Polymer 1105 Nanoparticles for Free Particle Diffusion in Cytosol. *Adv. Funct. Mater.* 1106 **2018**, *28*, 1805157.
- (81) Andreiuk, B.; Reisch, A.; Lindecker, M.; Follain, G.; Peyrieras, 1107 N.; Goetz, J. G.; Klymchenko, A. S. Fluorescent Polymer Nanoparticles 1108 for Cell Barcoding *in Vitro* and *in Vivo*. *Small* **2017**, *13*, 1701582.
- (82) Trofymchuk, K.; Reisch, A.; Didier, P.; Fras, F.; Gilliot, P.; Mely, 1109 Y.; Klymchenko, A. S. Giant Light-Harvesting Nanoantenna for Single- 1110 Molecule Detection in Ambient Light. *Nat. Photonics* **2017**, *11*, 657.

- 1129 (83) Severi, C.; Melnychuk, N.; Klymchenko, A. S. Smartphone-
1130 Assisted Detection of Nucleic Acids by Light-Harvesting FRET-Based
1131 Nanoprobe. *Biosens. Bioelectron.* **2020**, *168*, 112515
- 1132 (84) Egloff, S.; Melnychuk, N.; Reisch, A.; Martin, S.; Klymchenko, A.
1133 S. Enzyme-Free Amplified Detection of Cellular MicroRNA by Light-
1134 Harvesting Fluorescent Nanoparticle Probes. *Biosens. Bioelectron.* **2021**,
1135 *179*, 113084.
- 1136 (85) Melnychuk, N.; Ashokkumar, P.; Aparin, I. O.; Klymchenko, A. S.
1137 Pre- and Postfunctionalization of Dye-Loaded Polymeric Nanoparticles
1138 for Preparation of FRET-Based Nanoprobes. *ACS Appl. Mater.*
1139 *Interfaces* **2021**, DOI: [10.1021/acscpm.1c00819](https://doi.org/10.1021/acscpm.1c00819).
- 1140 (86) Andreiuk, B.; Reisch, A.; Bernhardt, E.; Klymchenko, A. S.
1141 Fighting Aggregation-Caused Quenching and Leakage of Dyes in
1142 Fluorescent Polymer Nanoparticles: Universal Role of Counterion.
1143 *Chem. - Asian J.* **2019**, *14*, 836–846.
- 1144 (87) Olie, R. A.; Simões-Wüst, A. P.; Baumann, B.; Leech, S. H.;
1145 Fabbro, D.; Stahel, R. A.; Zangemeister-Wittke, U. A Novel Antisense
1146 Oligonucleotide Targeting Survivin Expression Induces Apoptosis and
1147 Sensitizes Lung Cancer Cells to Chemotherapy. *Cancer Res.* **2000**, *60*,
1148 2805–2809.
- 1149 (88) Arvey, A.; Hermann, A.; Hsia, C. C.; Ie, E.; Freund, Y.; McGinnis,
1150 W. Minimizing Off-Target Signals in RNA Fluorescent *in Situ*
1151 Hybridization. *Nucleic Acids Res.* **2010**, *38*, e115.
- 1152 (89) Thomsen, R.; Nielsen, P. S.; Jensen, T. H. Dramatically
1153 Improved RNA *in Situ* Hybridization Signals Using LNA-Modified
1154 Probes. *RNA* **2005**, *11*, 1745–1748.
- 1155 (90) Floyd, D. L.; Ragains, J. R.; Skehel, J. J.; Harrison, S. C.; van
1156 Oijen, A. M. Single-Particle Kinetics of Influenza Virus Membrane
1157 Fusion. *Proc. Natl. Acad. Sci. U. S. A.* **2008**, *105*, 15382–15387.
- 1158 (91) Karstens, T.; Kobs, K. Rhodamine B and Rhodamine 101 as
1159 Reference Substances for Fluorescence Quantum Yield Measurements.
1160 *J. Phys. Chem.* **1980**, *84*, 1871–1872.
- 1161 (92) Texier, I.; Goutayer, M.; Da Silva, A.; Guyon, L.; Djaker, N.;
1162 Josserand, V.; Neumann, E.; Bibette, J.; Vinet, F. Cyanine-Loaded Lipid
1163 Nanoparticles for Improved *in Vivo* Fluorescence Imaging. *J. Biomed.*
1164 *Opt.* **2009**, *14*, 054005.

Supporting information

Amplified Fluorescence *in Situ* Hybridization by Small and Bright Dye-Loaded Polymeric Nanoparticles

Sylvie Egloff,[§] Nina Melnychuk,[§] Elisabete Da Silva, Andreas Reisch, Sophie Martin, Andrey S. Klymchenko*

Laboratoire de Bioimagerie et Pathologies, UMR 7021 CNRS, Faculté de Pharmacie, Université de Strasbourg, 74, Route du Rhin, 67401 Illkirch, France.

[§] These authors contributed equally to this work.

*Corresponding author. E-mail address: andrey.klymchenko@unistra.fr (A. S. Klymchenko); tel: +33 368 85 42 55.

Table S1. Fluorescence quantum yields (QY) of NPs prepared with different dyes at varied loading mass ratio (*vs.* polymer).

Encapsulated dye	Loading mass ratio (%) ^a	QY (%)
R18/F5	30	52
	50	41
	70	32
Rh101-C18/F5	20	34
	30	21
	50	10
Rh101-C18/F12	20	46
	30	34
	50	18
DiD/F12	20	45
	30	42
	50	32

^aThe weight% loading of the dye with respect to the polymer.

Table S2. Sizes of bare and DNA-functionalized NPs according to TEM and DLS data.^a

Dye	Type of NPs	Size by DLS	Size by TEM
Rh101-C18/F12	bare	17.0 ± 0.4	14.1 ± 1.8
	T20-NPs	23.4 ± 1.0	16.8 ± 2.0
R18/F5	bare	17.7 ± 0.4	18.2 ± 2.7
	T20-NPs	26.9 ± 0.3	20.0 ± 2.6
DiD/F12	bare	N/A	16.3 ± 2.3
	T20-NPs	N/A	17.9 ± 2.5

^a Error bars are standard deviation of the mean ($n \geq 3$ for DLS; at least 200 NPs were analyzed for TEM).

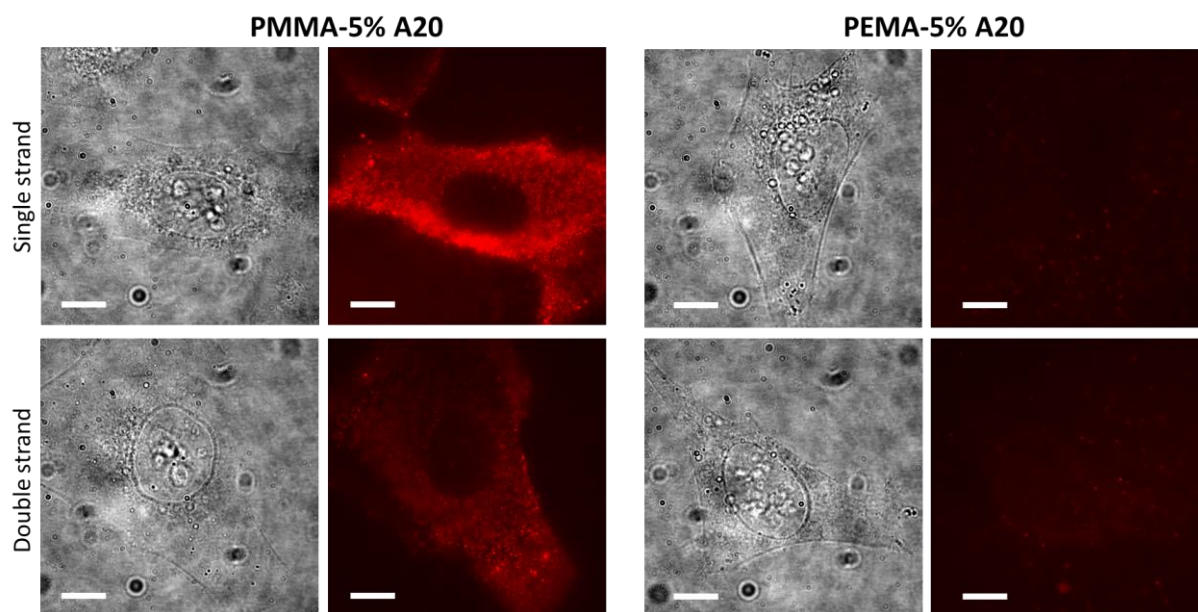


Figure S1. Effect of polymer nature and different grafted DNA sequences. Bright field (right) and fluorescence (left) images of fixed HeLa cells incubated with PMMA-based NPs and PEMA-based NPs of ~20 nm core size, functionalized with A20. Both single-stranded and double stranded (annealed with T20) DNA-NPs were tested (30 min incubation with cells). TIRF mode was used on fixed HeLa cells without washing. Scale bar: 10 μ m. PBS buffer with 50 mg/L Tween 80 was used for incubation and imaging.

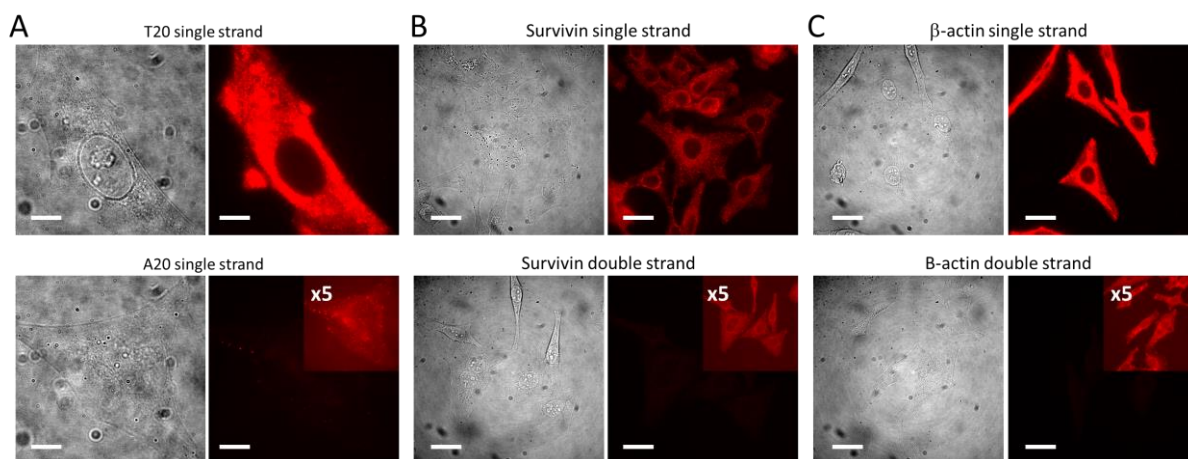


Figure S2. (A) Comparison of TIRF fluorescence images of PEMA-based NPs functionalized with T20 (upper panel) and A20 (lower panel) recorded at identical conditions (inset shows an image where signal was amplified 5-fold for visibility of the cell). Cells were incubated during 1 h with NPs, then washed two times with 0.1 % BSA / PBS. Scale bar: 10 μm . (B,C) Epi-fluorescence microscopy of fixed HeLa cells incubated for 1 h with DNA-NPs targeting survivin (B) and β -actin (C) (the same washing protocol as in A). Images for single-stranded (upper panels) and double-stranded (annealed with complementary strands) DNA-NPs are shown. Scale bar: 50 μm . PBS buffer with 50 mg/L Tween 80 was systematically used for incubation and imaging (A-C).

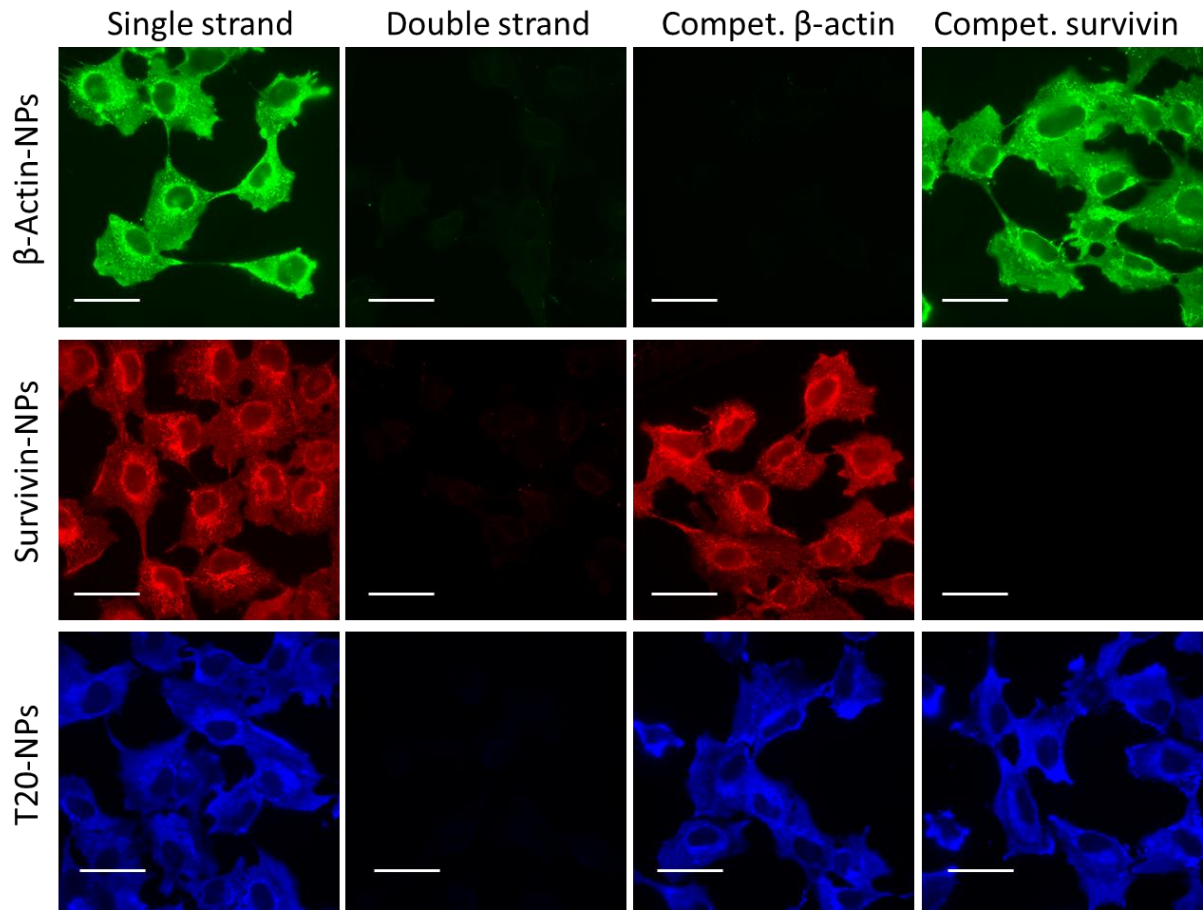


Figure S3. Validation of DNA-NPs for detection of intracellular mRNA targets in fixed U87 cells. Single stranded probes β -actin-NPs loaded with Rh110-C18/F12, survivin-NPs loaded with R18/F5 and A20-NPs loaded with DiD/F12 for β -actin, survivin and poly(A) sequences of mRNA, were compared to controls with double stranded DNA-NPs (annealed with complementary sequences) and competitor oligonucleotides (100 nM) for corresponding β -actin and survivin sequences added 1 h before addition of DNA NPs. DNA-NPs concentration expressed in encapsulated dyes was 100 nM. Scale bar: 50 μ m.

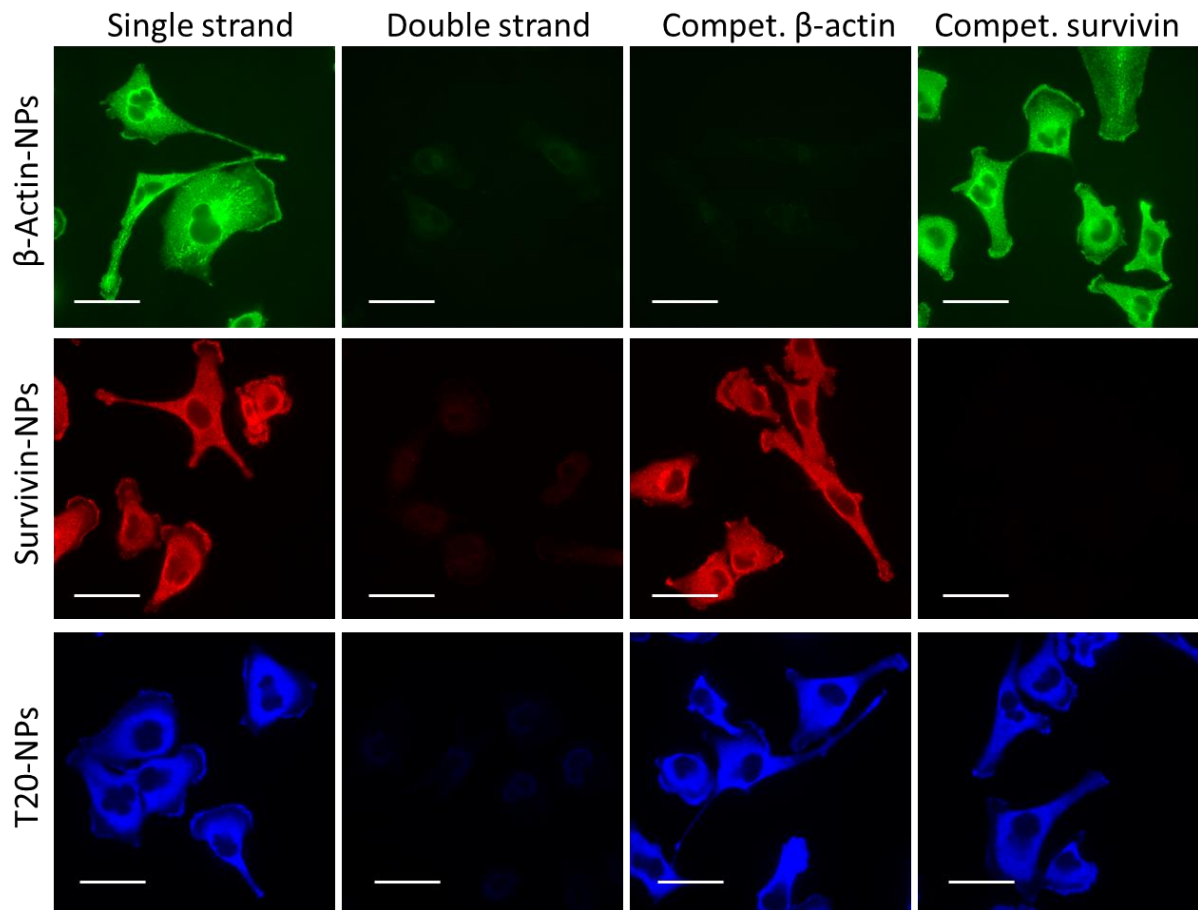


Figure S4. Validation of DNA-NPs for detection of intracellular mRNA targets in fixed MDA-MB-231 cells. Single stranded probes β -actin-NPs loaded with Rh110-C18/F12, survivin-NPs loaded with R18/F5 and A20-NPs loaded with DiD/F12 for β -actin, survivin and poly(A) sequences of mRNA, were compared to controls with double stranded DNA-NPs (annealed with complementary sequences) and competitor oligonucleotides (100 nM) for corresponding β -actin and survivin sequences added 1 h before addition of DNA NPs. DNA-NPs concentration expressed in encapsulated dyes was 100 nM. Scale bar: 50 μ m.

Table S3. Manders' colocalization coefficient M1/M2 of multiplexed detection of mRNA sequences.

Colocalization	HeLa	U87	MDA
Actin in T20	0.988	0.935	0.998
T20 in Actin	0.322	0.208	0.283
Survivin in T20	0.937	0.750	0.962
T20 in Survivin	0.275	0.208	0.437
Actin in Survivin	0.661	0.499	0.946
Survivin in Actin	0.678	0.330	0.604

Supporting videos

Video S1. Video of 3D reconstruction of surviving mRNA imaging using AmpliFISH probes. HeLa cells were incubated during 1 h with DNA-NPs targeting survivin, then washed two times with 0.1 % BSA / PBS. Multiple stacks were acquired using spinning disk microscopy. 3D image reconstruction was performed using IMARIS software. Gray dots correspond to NPs identified automatically by the imaging software for quantitative analysis.

Video S2. Real-time video imaging of HeLa cells stained with actin-NPs using spinning disk fluorescence microscopy. HeLa cells were incubated during 1 h with DNA-NPs targeting β -actin mRNA, then washed two times with 0.1 % BSA / PBS. Multiple images from a single plane of HeLa cells was recorded each 100 ms using spinning disk microscopy. Scale bar is 10 μ m.